Acta Biomaterialia 180 (2024) 154–170

Contents lists available at ScienceDirect

Acta Biomaterialia

journal homepage: www.elsevier.com/locate/actbio

Full length article

Gallium and silver-doped titanium surfaces provide enhanced osteogenesis, reduce bone resorption and prevent bacterial infection in co-culture

David Piñera-Avellaneda[a,b,c,*], Judit Buxadera-Palomero[a,b,c], Rosalia Cuahtecontzi Delint[d], Matthew J. Dalby[d], Karl V. Burgess[e], Maria-Pau Ginebra[a,b,c,f], Elisa Rupérez[a,b,c], José María Manero[a,b,c]

[a] Biomaterials, Biomechanics and Tissue Engineering Group, Department of Materials Science and Engineering, Technical University of Catalonia (UPC), Barcelona East School of Engineering (EEBE), 08019 Barcelona, Spain
[b] Barcelona Research Center in Multiscale Science and Engineering, UPC, EEBE, 08019, Barcelona, Spain
[c] Institut de Recerca Sant Joan de Déu, 08034, Barcelona, Spain
[d] Centre for the Cellular Microenvironment, Institute of Molecular, Cell and Systems Biology, College of Medical, Veterinary and Life Sciences, University of Glasgow, Glasgow, G12 8QQ, UK
[e] EdinOmics, University of Edinburgh, Max Born Crescent, Edinburgh, EH9 3BF, UK
[f] Institute for Bioengineering of Catalonia (IBEC), 08028, Barcelona, Spain

ARTICLE INFO

Article history:
Received 21 December 2023
Revised 5 April 2024
Accepted 11 April 2024
Available online 14 April 2024

Keywords:
Silver
Gallium
Titanium
Bone resorption
Antibacterial

ABSTRACT

Bacterial infection remains a significant problem associated with orthopaedic surgeries leading to surgical site infection (SSI). This unmet medical need can become an even greater complication when surgery is due to malignant bone tumor. In the present study, we evaluated *in vitro* titanium (Ti) implants subjected to gallium (Ga) and silver (Ag)-doped thermochemical treatment as strategy to prevent SSI and improve osteointegration in bone defects caused by diseases such as osteoporosis, bone tumor, or bone metastasis. Firstly, as Ga has been reported to be an osteoinductive and anti-resorptive agent, its performance in the mixture was proved by studying human mesenchymal stem cells (hMSC) and pre-osteoclasts (RAW264.7) behaviour. Then, the antibacterial potential provided by Ag was assessed by resembling "The Race for the Surface" between hMSC and *Pseudomonas aeruginosa* in two co-culture methods. Moreover, the presence of quorum sensing molecules in the co-culture was evaluated. The results highlighted the suitability of the mixture to induce osteodifferentiation and reduce osteoclastogenesis *in vitro*. Furthermore, the GaAg surface promoted strong survival rate and retained osteoinduction potential of hMSCs even after bacterial inoculation. Therefore, GaAg-modified titanium may be an ideal candidate to repair bone defects caused by excessive bone resorption, in addition to preventing SSI.

Statement of significance

This article provides important insights into titanium for fractures caused by osteoporosis or bone metastases with high incidence in surgical site infection (SSI) because in this situation bacterial infection can become a major disaster. In order to solve this unmet medical need, we propose a titanium implant modified with gallium and silver to improve osteointegration, reduce bone resorption and avoid bacterial infection. For that aim, we study osteoblast and osteoclast behavior with the main novelty focused on the antibacterial evaluation. In this work, we recreate "the race for the surface" in long-term experiments and study bacterial virulence factors (*quorum sensing*). Therefore, we believe that our article could be of great interest, providing a great impact on future orthopedic applications.

* Corresponding author: Barcelona East School of Engineering (EEBE), Av. Eduard Maristany 16, 08019 Barcelona, Spain.
E-mail address: david.pinera@upc.edu (D. Piñera-Avellaneda).

https://doi.org/10.1016/j.actbio.2024.04.019
1742-7061/

1. Introduction

Bacterial infection is one of the biggest issues in orthopaedic surgeries [1–3]. This problem becomes a major complication when the surgery is for a malignant bone tumor. In this case, opportunistic pathogens may take advantage of patient's immunodeficiency caused both by cancer treatment and the presence of the implant to provoke a surgical site infection (SSI) [4]. Indeed, SSI has an incidence almost 10 times higher in orthopaedic surgeries after bone tumor resection than normal orthopaedic surgeries [5,6] and leads to increased morbidity and mortality with associated costs [7]. Normally, when SSI occurs antibiotics are applied, but their excess use would be contributing to the increase of antibiotic-resistant bacteria [8–10]. Therefore, in order to solve this unmet medical need, Titanium (Ti) (or Ti alloys) implants, which are common dental and orthopaedic materials [11,12], need to ensure strong osteointegration to allow the patients' cells to strongly adhere to the implant instead of bacteria (race to the surface) resultant in biofilm formation [13].

In this regard, a thermochemical treatment developed by Kokubo [14], is a well-established strategy to enhance the bone-bonding ability in Ti implants. The thermochemical treatment creates a calcium titanate layer on the Ti surface that will be capable of forming apatite when is in contact with body fluids [15–17]. As apatite is a mineral component of the bone's extracellular matrix [18,19], a better and faster binding between implant and bone will be achieved. However, in some instances, such as cancer, accelerating the osteointegration process might not be enough to avoid bacterial infection.

For this reason, the thermochemical treatment has been modified with the addition of functional metal ions that can potentially prevent the development of SSI [20,21]. Among the possible ions, silver (Ag) has been used for its promising antibacterial activity [22–24] and its role as an antibacterial agent is clear [25–27]. Indeed, Ag has previously been incorporated into the calcium titanate and the release of Ag^{+} has displayed antibacterial activity [21]. The ability to introduce bioactive ions could have further benefit as, for example, by adding Gallium (Ga). Ga^{3+}, due to similarity with ferric ion (Fe^{3+}), can alter the iron metabolism and reduce osteoclastogenesis that is a problematic post bone cancer therapy due to ongoing bone loss [28,29]. Indeed, the reduction of bone resorption might also be beneficial in age related conditions such as osteoporosis [30].

Consequently, the objective of this work is to demonstrate that thermochemically treated Ti with Ag and Ga may improve osteointegration avoiding the emergence of SSI, especially in cases where resorption is a worry. Therefore, here, we test *in vitro* osteoblast and osteoclast differentiation and antibacterial activity. Firstly, human mesenchymal stem cells (hMSC) behaviour was evaluated in terms of cell adhesion, proliferation and differentiation. Secondly, RAW264.7 macrophages were tested for ability to form multinuclear cells, for tartrate-resistant acid phosphatase (TRAP) activity and for specific markers involved in osteoclastogenesis.

Finally, the antibacterial evaluation was made by simulating the race for the surface [13]. To better represent the real-world situation, a co-culture system of hMSCs and pathogenic, biofilm forming bacteria, *Pseudomonas aeruginosa* (*P. aeruginosa*) was used. *P. aeruginosa*, is a Gram negative, sepsis causing, pathogen commonly present in orthopaedic infections [31]. Further, it was selected for experiments as its quorum signalling is well understood and we have a panel of *P. aeruginosa* quorum signalling molecule (QSM) standards for mass spectrometry taken from [32]. In this work, we used a bacteria first (2 h seeded before hMSC addition) and hMSC first (24 h seeding before bacterial addition) approach to represent different winners of the race to the surface and assess the outcome, with the different seeding times representing the different attachment speeds of the bacteria and hMSCs (Fig. 1). Throughout the co-culture, cell adhesion, morphology, viability, apoptosis and differentiation assays were assessed. Moreover, as homoserine lactones are crucial molecules for intracellular signalling in bacteria because they monitor their population density in *quorum sensing* manner [33], the content of these QSMs present in *P. aeruginosa*

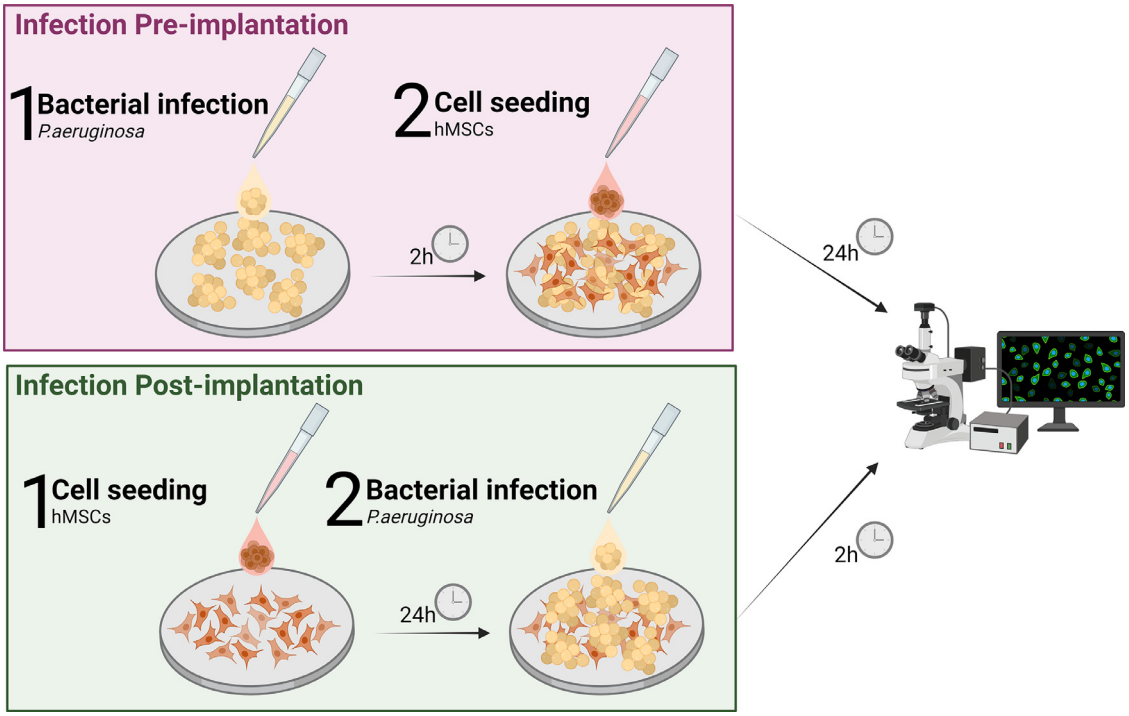

Fig. 1. Scheme of the two co-culture systems carried out in this work. The method "infection pre-implantation" mimics the scenario in which the implant is inserted in a previously infected bone tissue and the method "infection post-implantation", when infection occurs after orthopaedic surgery. Based on Piñera-Avellaneda, D. et al. [21].

after being exposed to our samples were analysed by mass spectrometry.

2. Materials and methods

2.1. Materials

Commercially pure Ti grade 2 solid discs of 10 mm diameter and 2 mm thickness were used for the *in vitro* characterization. Ti discs were polished with SiC grinding papers (P800 and P1200) and subsequently a colloidal silica suspension of 0.05 μm. Before their use, Ti samples were ultrasonically cleaned with acetone, 2-propanol and distilled water twice for 5 min each, and finally stored dried with N_2.

2.2. Thermochemical treatment

The thermochemical treatment was made by following the procedure reflected in Table 1 [34].

2.3. Surface characterization

Ion release. The release of Ga^{3+} from the treated simples was evaluated according to ISO-10993-12 standard by using and inductively coupled plasma mass spectrometry (ICP-MS, Agilent 5100 SVD ICP-OES, CA, USA). Each sample was immersed Mili-Q water (1 mL of Mili-Q water per 0.2 gram of sample), after each time point, 1 mL of the suspension was taken, filtered and diluted 1:10 in 2 % nitric acid. Same volume was replaced with fresh medium.

X-ray photoelectron spectroscopy (XPS). XPS experiments were performed in a SPECS system with a PHOIBOS 150 EP hemispherical energy analyzer with MCD-9 detector, using an X-ray source Al Kα line of 1486.6 eV energy and 150 W power and using a pass energy of 20 eV, placed at 54° respect to the analyzer axis and calibrated by the 3d5/2 line of Ag with a full width at half maximum (FWHM) of 1.211 eV. Survey spectra were recorded at an energy step of 1 eV, and high-resolution spectra at 0.1 eV.

2.4. In vitro *cell evaluation in mono-culture*

Cell culture. hMSCs (ATCC, USA) were cultured in Advanced Dulbecco's Modified Eagle Medium with D-glucose, nonessential amino acids, sodium pyruvate and supplemented with 10 % foetal bovine serum (FBS), 1 % penicillin/streptomycin (50 U/mL and 50 μg/mL, respectively) and 20 mM N-(2-hydroxyethyl)piperazine-N′-ethanesulfonic acid buffer solution, all from Gibco™. Mouse monocyte macrophages RAW 264.7 cells (ATCC, USA) were cultured in Dulbecco's Modified Eagle Medium supplemented with 10 % FBS, 1 % penicillin/streptomycin (50 U/mL and 50 μg/mL, respectively) and 20 mM N-(2-hydroxyethyl) piperazine-N′-ethanesulfonic acid buffer solution, all from Gibco™. Cells were maintained and expanded at 37 °C in a 95 % humidified atmosphere containing 5 % of CO_2. Cell density and passage are indicated in each particular experiment.

Sample sterilization and incubation. Solid discs of Ti, both treated and untreated (control) were sterilized by washing them in ethanol (70 %, v/v) for 20 min, and then rinsed thrice with PBS. After that, the samples were incubated in cell culture medium for 72 h at 37 °C.

hMSC adhesion and morphology assay. hMSCs at passage 4 were seeded on Ti surfaces at a density of 15,000 cells per sample, and incubated for 24 h at 37 °C. After incubation, cell medium was removed and the samples were rinsed with 500 μL of PBS, then cells were fixed with 500 μL of 4 % of paraformaldehyde (Sigma) for 20 min at RT. After fixation, samples were washed thrice with 20 mM glycine in PBS (PBS-Gly) for 5 min. Then, cells were permeabilized with 0.05 % Triton X-100 in PBS for 20 min at RT, rinsed thrice again with PBS-Gly, and blocked with 1 % BSA in PBS for 30 min. Then, the medium was removed and the cells were incubated with primary antibody mouse anti-vinculin (V9131, Sigma-Aldrich, USA) (1:400 in 1 % bovine serum albumin (BSA) in PBS). After incubation, samples were washed thrice with PBS-Gly-and incubated with secondary antibody Alexa Fluor 488 goat anti-mouse IgG (R37120, Invitrogen, USA) for 1 h in the dark following manufacturing protocol. After that, samples were washed with PBS-Gly-and incubated with Alexa Fluor 546 Phalloidin-Rhodamine (A22283, Invitrogen, USA) (1:400 in PBS-0.05 % triton) during 1 h in dark. Samples were washed thrice with PBS-Gly-and DAPI (1:1000 in PBS-Gly) was added for 2 min in the dark. After incubation, the samples were finally rinsed with PBS-Gly-and ready for image analysis. Randomized images of each sample were captured using Zeiss LSM 800 (Zeiss, Germany) and analyzed with Fiji/ImageJ [35].

hMSC proliferation assay. hMSCs at passage 4 were seeded on Ti surfaces at 15,000 cells per sample and maintained in culture for 1, 7, 14 and 21 days, changing the medium twice or thrice a week. After each incubation period the cells were rinsed thrice in 500 µL PBS and incubated with 350 µL 10 % of PrestoBlue™ (Invitrogen, USA) for 1 h at 37 °C. As a negative control, PrestoBlue™ was incubated without cells. Then, 100 μL of the medium was transferred to a black 96-well plate to measure the excitation wavelength at 560 nm and emission at 590 nm using Synergy HTX multimode reader (Bio-Tek, USA).

hMSC Alkaline phosphatase (ALP) activity. ALP activity of the cells in the proliferation assay was assessed on days 14 and 21. Cells were rinsed with 500 µL PBS and then lyzed with 500 µL of mammalian protein extraction reagent (M-PER, Thermo Fisher Scientific, USA). Samples were incubated for 1 h at 37 °C using the SensoLyte pNPP Alkaline Phosphatase Assay Kit (AnaSpec Inc., USA) and the absorbance was registered at 405 nm using a Synergy HTX multimode reader (Bio-Tek, USA). The resulting ALP quantity was expressed as ng/mL and normalized to the cell number obtained in cell proliferation assay.

hMSC mineralization assay. hMSCs were seeded at passage 4 on Ti surfaces at 20,000 cells per sample for 21 days. After each incubation time, cell medium was removed and the samples were rinsed with PBS, then cells were fixed with 4 % paraformaldehyde (Sigma) for 20 min at RT. After that, samples were rinsed twice with Milli-Q water and calcium deposits were stained with 500 µL/sample of 40 mM Alizarin Red S (Sigma-Aldrich) for 20 min with gentle shaking. Unincorporated dye was removed and washed with Milli-Q water until the medium became clear. Then, 6 randomized images of each sample were captured using an Olympus BX51-P bright-field microscope (Olympus Corp., Japan). Quantification of calcium deposits was performed with Fiji/ImageJ [35].

Table 1
Stages of thermochemical treatments performed and samples references.

Sample	First step	Second step	Thrid step	Fourth step
Ga10	5 M NaOH 24 h/60 °C	100 mM $CaCl_2$ + 10 mM $Ga(NO_3)_3$ 24 h/40 °C	Heat treatment 600 °C/1 h	H_2O treatment 24 h/80 °C
Ag	5 M NaOH 24 h/60 °C	100 mM $C_4H_6CaO_4$ + 1 mM $AgNO_3$ 24 h/40 °C	Heat treatment 600 °C/1 h	H_2O treatment 24 h/80 °C
GaAg	5 M NaOH 24 h/60 °C	100 mM $C_4H_6CaO_4$ + 2 mM $AgNO_3$ + 20 mM $Ga(NO_3)_3$ 24 h/40 °C	Heat treatment 600 °C/1 h	H_2O treatment 24 h/80 °C

Table 2
Osteogenic primer sequences used for RT-PCR.

Gene	Forward Sequence (5′to3′)	Reverse Sequence (5′to3′)
β-ACTIN	TTGCCATCAATGACCCCTTCA	CGCCCCACTTGATTTTGG A
RUNX2	AAATGCCTCCGCTGTTATGAA	GCTCCGGCCCACAAATCT
COL1A1	AGGTCCCCCTGGAAAGAA	AATCCTCGAGCACCCTGA
ALP	ATCTTTGGTCTGGCTCCCATG	TTTCCCGTTCACCGTCCAC
OPN	AGCTGGATGACCAGAGTGCT	TGAAATTCATGGCTGTGGAA

hMSC osteogenic expression. hMSCs were seeded at passage 3 on Ti surfaces at 30,000 cells per sample for 3 and 7 days in order to evaluate gene expression. After each time point, cells were detached and centrifuged and pellets collected. Then, cells were lyzed and total RNA was extracted and purified using RNeasy Mini Kit columns (Qiagen, Hilden, Germany) as described in the manufacturer's instructions. Then, cDNA synthesis was performed using the Maxima First Strand cDNA Synthesis Kit for qRT-PCR, with dsDNase (Thermo Scientific, # K1671). RT-PCR was carried out on a Mic real time PCR cycler (Bio Molecular Systems, Australia) and gene expression was assessed by QuantiNova Fast SYBR™ Green PCR Master Mix (Qiagen). β-ACTIN was used as a housekeeping gene and the relative gene expression levels were evaluated using $2^{\Delta\Delta\text{-Ct}}$ method. Primer sequences used are shown in Table 2.

Multinuclearity study of RAW264.7 cells. RAW264.7 cells were seeded on Ti surfaces at 10,000 cells per sample. The medium used for the seeding was supplemented with RANKL (60 ng/mL) and maintained in culture for 4 and 6 days, changing the medium once and thrice, respectively. After incubation time, the fluorescence staining was carried out following the procedure explained above.

TRAP staining. RAW264.7 cells were seeded on Ti surfaces at 10,000 cells per sample. The medium used for the seeding was supplemented with RANKL (60 ng/mL) and maintained in culture for 6 days, changing the medium thrice. After incubation time, the medium was removed, and samples rinsed with PBS. Then, the samples were stained using leukocyte acid phosphatase (TRAP) kit (Sigma-Aldrich, USA) following the provided procedure. After 1 h of incubation, the samples were thoroughly rinsed with deionized water and then, haematoxylin solution was added for staining the nuclei. Then, samples were rinsed in alkaline tap water, dried, and evaluated using an Olympus BX51-P bright-field microscope (Olympus Corp., Japan).

RAW264.7 osteoclastic expression. RAW264.7 cells were seeded on Ti surfaces at 10,000 cells per sample. The medium used for the seeding was supplemented with RANKL (60 ng/mL) and maintained in culture for 4 days, changing the medium twice. RNA extraction and RT-PCR were carried out following the procedure explained above. GAPDH was used as a housekeeping gene and the relative gene expression levels were evaluated using $2^{\Delta\Delta\text{-Ct}}$ method. Primer sequences used are shown in Table 3.

2.5. In vitro *co-culture evaluation*

Bacteria and hMSC were co-cultured in two different methods (Fig. 1) as were published in Pinera-Avellaneda, D. et al. [21] hMSC (PromoCell C12974) at passage 2–3 were cultured in DMEM (Sigma) supplemented with 10 % FBS (Sigma), 1 % (v/v) L-glutamine (200 mM, Gibco), 1 % sodium pyruvate (11 mg/mL, Sigma), 1 % non-essential amino acids (MEM NEAA, Gibco) and 1 % antibiotics. *Pseudomonas aeruginosa* (*P. aeruginosa* ATCC 27853) bacterial strain was employed for this experiment. *P. aeruginosa* was grown aerobically overnight in DMEM at 37 °C in a shaker incubator at 220 RPM. Then, bacterial suspension was diluted in DMEM to $OD_{600} = 0.1$ and incubated to reach the mid-exponential phase (approx. 10^8 CFU/mL). Sample sterilization and incubation were required following the procedure previously described.

Method of co-culture "infection pre-implantation". 10^3 CFU of *P. aeruginosa* were inoculated to each Ti sample and incubated for 2 h at 37 °C. After incubation, hMSC in antibiotic-free cell medium with 1 % FBS were seeded on the samples at 30,000 density and incubated for 24 h at 37 °C and 5 % CO_2.

Method of co-culture "infection post-implantation". hMSC were seeded on Ti surfaces at density of 30,000 cells and incubated for 24 h at 37 °C. After incubation, cell medium was removed and samples were rinsed thrice with PBS. Then, 10^3 CFU of *P. aeruginosa* were inoculated. Finally, antibiotic-free cell medium with 1 % FBS was added to each sample and were incubated for 2 h at 37 °C and 5 % CO_2.

Cell adhesion *and morphology in co-culture.* Fluorescence staining was made as indicated in Section 2.4. Randomized images of each sample were captured using Zeiss LSM 980 (Zeiss, Germany) and analyzed with Fiji/ImageJ [35].

Annexin V immunofluorescence assay. After fluorescence staining, samples were washed thrice with PBS for 5 min. Then, cells were blocked with 1 % BSA in PBS for 30 min. After incubation, the medium was removed and cells were incubated with the primary antibody mouse annexin V (ab13196) (1:400 in 1 % BSA in PBS) for 1 h. After that, samples were washed thrice with PBS and incubated with secondary antibody horse anti rabbit IgG ($H + L$) BA-1100 (1:100 in 1 % BSA in PBS) for 1 h at 37 °C in the dark. Then, samples were washed with PBS and streptavidin-FITC fluoresceine (SA-5001) (1:100 in 1 % BSA in PBS) was added for 30 min at 4 °C. Finally, samples were washed with PBS. Randomized images of each sample were captured using Zeiss LSM 980 (Zeiss, Germany).

Flow cytometry. After the time required for the co-culture systems, cells were harvested by adding trypsin, washed with PBS and 1x Annexin V binding buffer (Annexin V V13241) was applied. Cells were incubated with Annexin V staining for 15 min in dark at RT. 500 µL of binding buffer were added to wash the cells and samples were centrifugated at 419 g for 4 min. Fresh 200 µL of binding buffer were added and 1 µL of Propidium Iodide (PI, V13245) before flow cytometry was performed. For positive Annexin V control, cells were subjected to 50 °C for 5 min and for positive PI control, cells were subjected to 50 °C for 15 min. The excitation/emission for Annexin V is 494/518, and 535/617 for PI. First, standard compensation was applied and then gating was performed using unstained cells using FSC-A vs SSC-A to include whole cells, then for single cells using FSC-a vs FSC–H. Necrotic, early apoptotic and dead cells were gated using a quadrant gate with Annexin V on the x axis, and PI on the Y axis (Attune NxT, Thermo fisher Scientific). Data analysis was done using FlowJo (BD biosciences).

Mineralization assay in co-culture. After 24 h, the time required by the co-culture experiments, medium was removed and fresh cell medium supplemented with 1 % penicillin/streptomycin was applied changing medium each 2–3 days. The co-culture was kept for 21 days. After that time, the mineralization assay was carried out following the procedure explained in Section 2.4. Six randomized images of each sample were captured using a Stemi 508 Stereo Microscope (ZEISS). Quantification of calcium deposits was performed with Fiji/ImageJ [35].

Metabolomics. After 24 h of co-culture, supernatant was collected and centrifuged for 15 min 14,000 rpm. The pellet was resuspended in 1 mL of buffer extraction composed by chloroform, ethanol and ddH_2O (1:3:1) and transferred to tubes with 0.1 mm acid washed glass beds kept in ice. Samples were then placed on a cell disrupter (Disrupter Genie bead beater, Scientific industries Inc., New York, USA) at 3000 rpm, for 30 s five times. Then, samples were centrifugated 15 min 14,000 rpm at 4 °C. The supernatant was transferred to new tubes and stored at

Table 3
Osteoclastic primer sequences used for RT-PCR.

Gene	Forward Sequence (5′to3′)	Reverse Sequence (5′to3′)
GAPDH	TGTGTCCGTCGTGGATCTGA	TTGCTGTTGAAGTCGCAGGAG
NFATc1	GGTAACTCTGTCTTTCTAACCTTAAGCTC	GTGATGACCCCAGCATGCACCAGTCACAG
TRAP	TACCTGTGTGGACATGACC	CAGATCCATAGTGAAACCGC
c-Fos	CCAAGCGGAGACAGATCAACTT	TCCAGTTTTTCCTTCTCTTTCAGCAGAT
MMP9	TCCAGTACCAAGACAAAGCCTA	TTGCACTGCACGGTTGAA

−80 °C. Metabolomic technique was carried out using an Agilent 1290 Infinity II series ultra-high performance liquid chromatography system coupled to an Agilent 6560 ion mobility quadrupole time-of-flight mass spectrometer with a Dual Agilent Jet Stream (AJS) electron ionization source (ESI). Chromatographic separation was performed using a ZORBAX Extend-C18 rapid resolution HT 2.1 × 50 mm, 1.8-micron column (Agilent Technologies 727700-902, Santa Clara CA). The solvent system consisted of MS-grade water with 0.1 % formic acid as solvent A and MS-grade acetonitrile with 0.1 % formic acid as solvent B. The solvent gradient was set to a constant flow rate of 0.150 mL/min starting at 90 % of solvent A, which was maintained for 1 min. The gradient was dropped to 50 % of solvent A at 1.5 min and to 1 % of solvent A at 5.5 min, where it was maintained until 7 min. The gradient was increased back to starting conditions of 90 % solvent A at 7.9 min, where it remained until 9.9 min. The column was maintained at a constant temperature of 40 °C throughout the run. 5 µl of each sample was injected into the column for analysis, and a quality control sample (generated by pooling equal volumes of each extract) was injected after every five samples to monitor instrument performance throughout data acquisition. Data was acquired in positive ionization mode by scanning a mass range of 50–1500 *m/z* with an acquisition rate of 1 spectra/s. The Dual AJS ESI gas temperature was maintained at 325 °C at a flow rate of 13 L/min. The nozzle voltage was set to 2000 V and VCap to 3750 V. A comprehensive list of ion mobility mass spectrometry parameters can be found in [36]. Data acquisition and processing were performed using the Agilent MassHunter software suite. Standards were run alongside the samples and $[M + H]^+$ ion species were used to identify the HSLs, using accurate mass, drift time, collision cross section and chromatographic retention time parameters.

In-cell western blot. After 24 h of co-culturing cells were fixed with 4 % PFA and PBS-triton was added to permeabilize. Then, PBS with 1 % powder milk was applied to block for 1 h and 30 min in shaking motion at room temperature. After blocking, primary antibody (RUNX2 M-70 sc-10758 rabbit polyclonal and osteonectin SPARC D2 sc-398419 mouse monoclonal) was added and kept overnight at 4 °C. Next day, the samples were rinsed using 0.1 % Tween-20/ PBS and secondary antibody (goat anti-rabbit 926-32211 IR dye 800, and goat anti-mouse 926–68070 IR dye 680) in blocking buffer was added along with CellTag IR 520 for 1 h at room temperature. Samples were rinsed as before and dried overnight at 4 °C. Then, fluorescence intensity of the protein expression was read using Odyssey M with 700, 800 and 520 laser. The data was analyzed using Empiria studio 2.0 software.

2.6. Statistical analysis

The statistical analysis was carried out by Minitab 19 software (Minitab, EE.UU), which was used to analyze whether statistically significant differences exist among the results or not. All samples were previously analyzed to determine if they followed a normal distribution by normality test. Then, ANOVA test or Kruskal-Wallis test were run to work out its p-value, depending if variable were normally distributed or not, respectively. Triplicates of each sample were used ($n = 3$). Each character represents significantly differences respect to the other ones for each time-point (p-value < 0.05).

3. Results

3.1. Ag^+ and Ga^{3+} are released from the GaAg-treated titanium surface

GaAg-treated Ti released Ag^+ especially fast in the first hours (Fig. 2a) reaching 47.95 ppb after 336 h (14 days). However, the release of Ga^{3+} was slower and lower, reaching 4.3 ppb after 336 h (Fig. 2b). Regarding XPS, percentage of atomic O, Ti, Ca, Ag and Ga present in each treated sample is found in Table 4. XPS analysis revealed the successful incorporation of Ga^{3+} and Ag^+ on the Ti surface.

3.2. The combination of Ga and Ag improves hMSC performance on Ag

Cells showed adequate spreading on the surfaces (Fig. 3a). The highest number of cells was found on the surface of Ga10 and the lowest on Ag (Fig. 3b). The reduction of number of cells by Ag was almost 45 % compared to Ti. Cell number on GaAg was higher than Ag, however, no significant differences were found between GaAg and Ti. Cell area was similar on Ti, Ga10 and GaAg (Fig. 3c), but on Ag, cell area was 20 % lower than the control. Focal adhesions were found in cells on all conditions (Fig. 3d). Regarding cell proliferation (Fig. 3e), Ag showed the lowest proliferation on day 1 compared to the other samples. Proliferation for GaAg was lower on day 14, but had caught up by day 21.

3.3. GaAg-treated titanium displays a similar osteodifferentiation profile than Ga10

ALP activity (Fig. 4a), an enzyme involved in bone mineralization [37], was only seen on Ga containing samples, Ga10 and GaAg on day 14. On day 21, the Ga samples still expressed high ALP activity and on the Ag sample began to be noted. Regarding cell mineralization measured by Alizarin red (Fig. 4b), the Ga samples (Ga10 and GaAg) gave significantly more mineral expression than Ti and Ag samples (Fig. 4c).

Regarding osteogenic markers, RUNX2 (osteoblast specific transcription factor [38]) was strongly upregulated by all treated samples on day 7 (Fig. 4d). Ga10 and GaAg upregulated its expression 4 times more than Ti, but the Ag samples were not able to induce

Table 4
Percentage of atomic O, Ti, Ca, Ag and Ga present in each treated sample.

	Ti	Ga10	Ag	GaAg
C 1 s	33.63 ± 2.93	26.60 ± 3.18	32.80 ± 8.61	40.21 ± 7.67
O 1 s	49.85 ± 1.56	52.89 ± 0.57	44.95 ± 3.66	43.58 ± 5.24
Ti 2p	8.79 ± 0.08	15.68 ± 2.14	14.68 ± 3.53	11.24 ± 1.21
Ca 2p	7.71 ± 1.44	2.30 ± 0.10	3.03 ± 0.48	0.85 ± 0.33
Ga 2p $_{3/2}$	0.02 ± 0.01	2.48 ± 0.40	0.00 ± 0.00	1.14 ± 0.60
Ag 3d	0.01 ± 0.01	0.07 ± 0.04	4.56 ± 0.94	3.01 ± 0.28

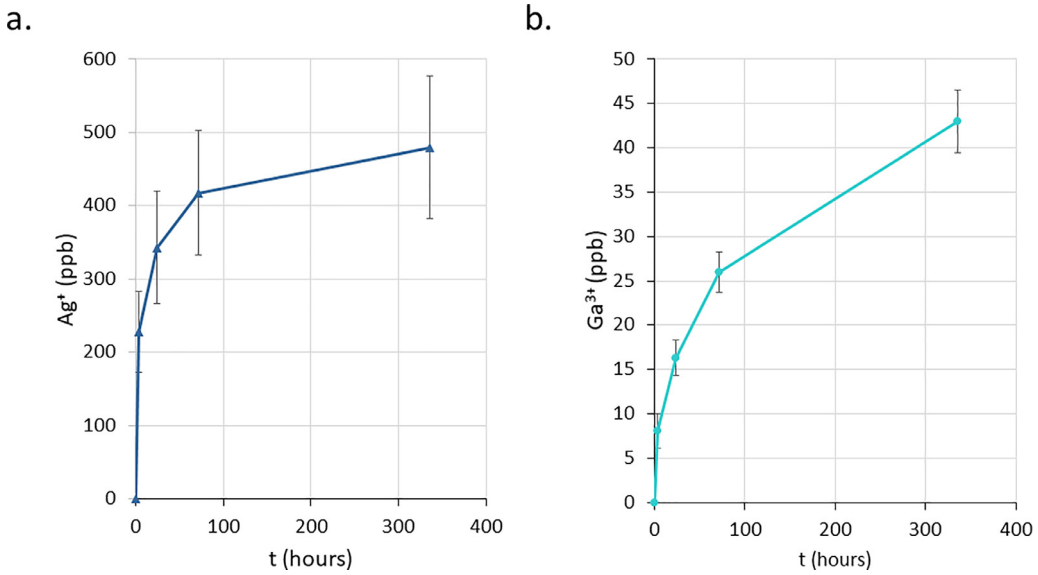

Fig. 2. Ion release from GaAg-treated titanium. (a) Accumulative curves of Ag^{+} release from the surface of GaAg-treated samples. (b) Accumulative curves of Ga^{3+} release from the surface of GaAg-treated samples.

the same upregulation. About COL1A1 (extracellular matrix protein highly expressed in bone and other tissues [39]) (Fig. 4e), no significant differences were found on day 3, however, the treated samples upregulated its expression on day 7. Regarding ALP (Fig. 4f), although no significant differences were found between the control and Ga-containing samples, its expression was downregulated by Ag on day 3. On day 7, treated samples upregulated its expression but on Ag was lower. Finally, regarding OPN (Fig. 4 g) (osteospecific extracellular matrix protein [40]), no significant differences were found on any condition.

3.4. GaAg-treated titanium reduces osteoclastogenesis

RANKL-induced RAW264.7 (RANKL induces macrophage fusing to osteoclasts [41]) cells were cultured on sample surfaces (Fig. 5a). On day 4, a few multinucleated cells were found on Ti. However, no evidence of multinucleated cells was found on the treated surfaces. On day 6, giant multinucleated cells were clearly found on Ti, while on Ag, multinucleated cells appeared under cell colonies (marked with yellow arrow in Fig. 5a). No evidence of multinucleated cells were found on Ga-containing samples. In order to further investigate this trend, TRAP staining was performed (Fig. 5b). TRAP-positive osteoclasts were clearly found on Ti and Ag samples. However, no evidence of osteoclasts was apparent on Ga10 and GaAg.

Regarding osteoclastic gene expression, NFATc1 (main transcription factor involved in osteoclastogenesis [42]) (Fig. 5c) was downregulated by Ga10 respect to Ti. However, GaAg did not show significant differences respect to Ti and Ga10. Moreover, Ag upregulated NFATc1 expression. About c-fos (involved in the autoamplification of the NFATc1 signal [43]) (Fig. 5d), while Ag upregulated its expression, no significant differences were found between Ti, Ga10 and GaAg. Concerning TRAP (Fig. 5e), its expression was strongly up-regulated by Ag. However, on GaAg its expression did not show significant differences when compared to both Ti and Ga10 samples. Finally, matrix metalloproteinase 9 (MMP9, produced by mature osteoclast [44]) expression (Fig. 5f) was dramatically downregulated by Ga10 up to 80 %. GaAg were also able to reduce its expression over 50 %. MMP9 showed higher expression on Ti and Ag.

3.5. GaAg-treated titanium maintains adequate cell adhesion and morphology after bacterial infection

With the *pre-implantation infection* method (Fig. 6a), after bacterial infection, hMSC morphology was dramatically compromised on Ti and Ga10 compared to monoculture (MC). Cells on Ag and GaAg were well spread in co-culture, although appearing smaller than in MC. In terms of cell adhesion (Fig. 6b), cells were hardly found on Ti and Ga10. In contrast, around 21,000 cells/cm^2 and 27,800 cells/cm^2 were found on Ag and GaAg, respectively. Moreover, cell area was drastically decreased on Ti and Ga10 (Fig. 6c). Further, the fluorescence intensity of the apoptosis marker Annexin V (Fig. 5d) was higher on Ti and Ga10 in co-culture than on Ag and GaAg.

With the *post-implantation* method (Fig. 7a), hMSCs were strongly affected by the presence of bacteria on Ti and Ga10. While more cells were visible than with the *pre-implantation* on the non-Ag containing samples, cell attachment (Fig. 7b) and spreading (Fig. 7c) was strongly reduced. hMSCs on Ag and GaAg were numerous and well spread (Fig. 7a-c). Looking at apoptosis, Annexin V (Fig. 7d) was more intense on Ti and Ga10 in co-culture than on Ag and GaAg.

3.6. GaAg-treated titanium achieves hMSC survival after bacterial infection

At this point, only Ag samples were taken forwards for more in-depth analysis as viability on non-Ag samples was clearly massively compromised and therefore, not worth taking forwards. Looking more closely at cell death with annexin V/propidium iodide co-staining and flow cytometry, viable, apoptotic and necrotic hMSCs could be identified in the infection models. The gating strategy for the *pre-implantation method* (Fig. 8a, b) showed the viability of hMSCs (Fig. 8c) around 60 % on Ag and 45 % on GaAg. No significant differences were found in necrotic cells; however, the number of early and late apoptotic cells were higher on GaAg.

Regarding the *post-implantation method*, the gating strategy (Fig. 8d, e) did not unveil significant differences in the number of viable, necrotic, early and late apoptotic cells between conditions (Fig. 8f). In this case, the cell viability was around 65 % in both Ag-doped samples.

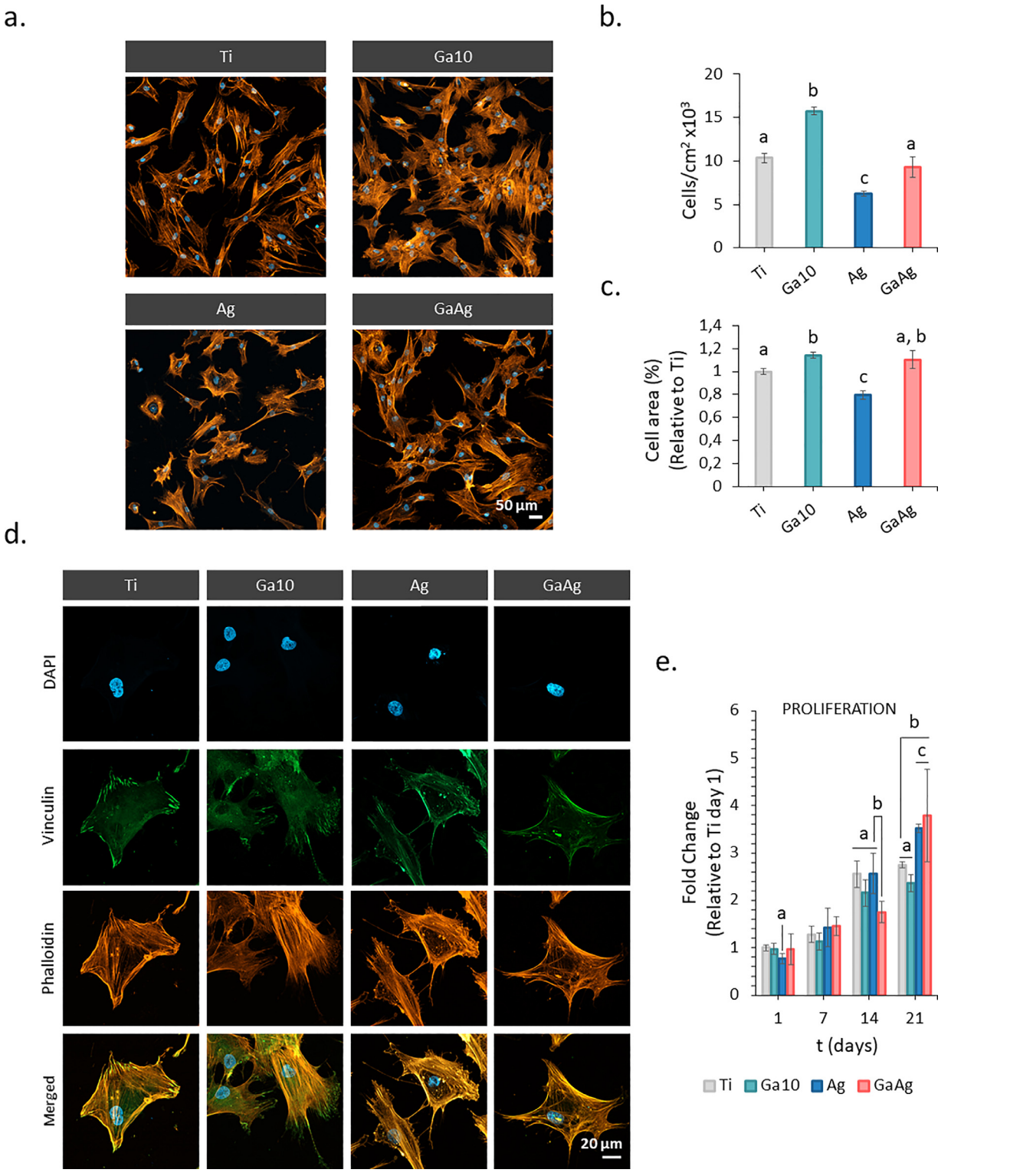

Fig. 3. Adhesion, morphology and proliferation of hMSC on mono-culture. (a) Representative images of hMSCs after 24 h by using fluorescence staining. Cells were labelled with DAPI (nuclei, blue) and phalloidin (F-actin, orange). (b) Quantification of cell number per cm^2 after 24 h. (c)% of area covered by cells area after 24 h. Six images per sample were used for quantification. Triplicates of each sample were used ($n = 3$). (d) hMSCs morphology after 24 h. hMSCs were labelled with DAPI (nuclei, blue), phalloidin (F-actin, orange) and vinculin (focal adhesions, green). (e) Proliferation of hMSCs for 21 days. Each character represents significantly differences respect to the other ones for each time-point (p-value < 0.05).

3.7. GaAg-treated surface protects cells from QSMs

Using an in-house panel of QSM standards linked to mass spectrometry [45], QSMs present in *P. aeruginosa* after being exposed to Ti, and Ti doped with Ag, and GaAg in both *pre- and post-* implantation models for 24 h were analysed (Fig. 9). To achieve this, we used choloform:methanol:water extraction with bead-beating to break the bacterial open and extract metabolites. Overall, homoserine lactone QSMs seemed to be downregulated in the *post-implantation* model compared to Ti only. This was most notable

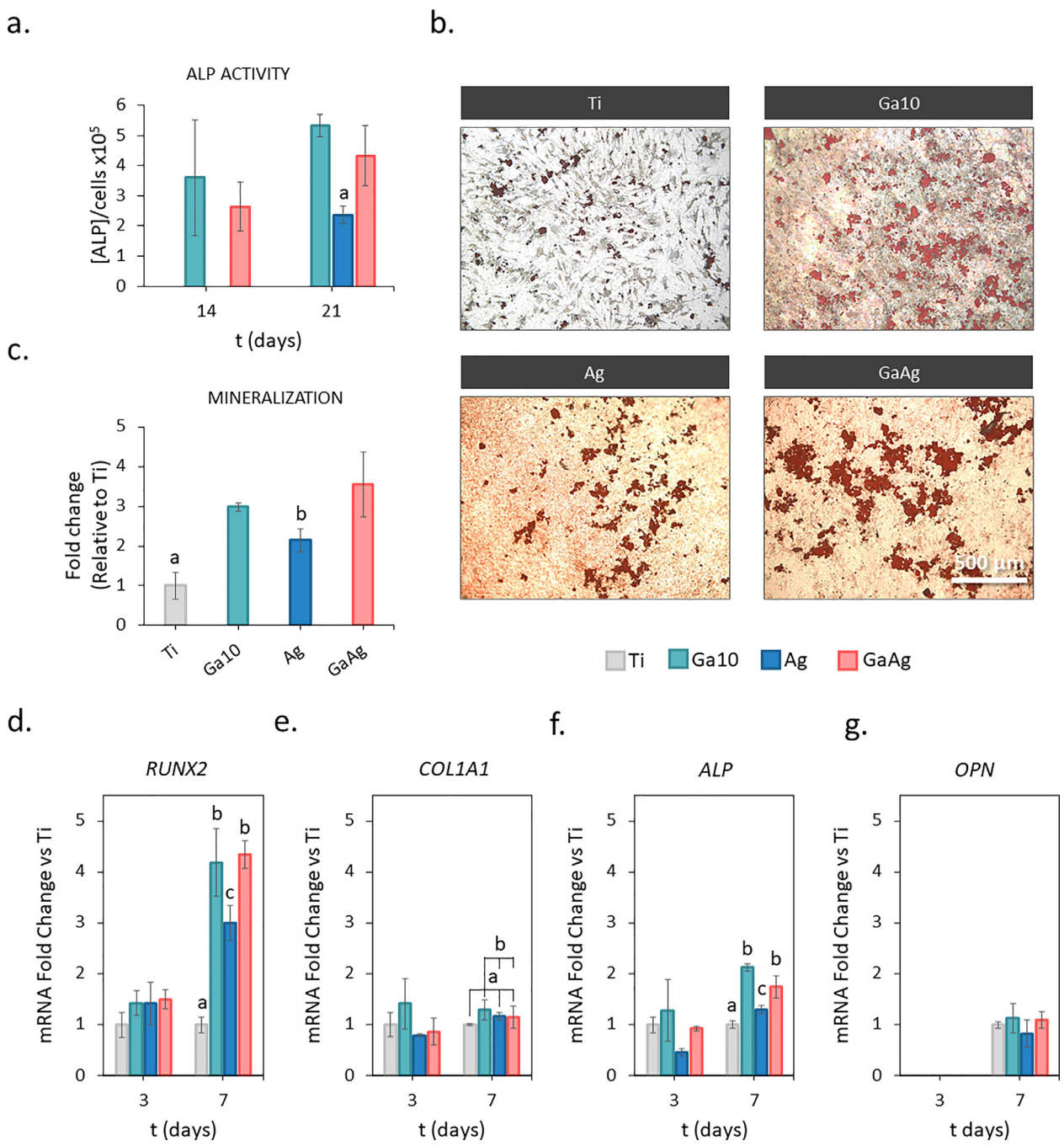

Fig. 4. Impact of Gallium-Silver coating in osteoblast differentiation on mono-culture. (a) ALP activity of hMSCs days 14 and 21. (b) Representative images of calcium deposits produced on day 21. Calcium deposits were labelled in red using Alizarin Red Staining. (c) Quantification of the calcium deposits. Results were expressed as fold change to Ti. Six images per sample were used to quantify. RT-PCR analyses of: (a) RUNX2 (b) COL1A1 (c) ALP and (d) OPN for hMSCs on days 3 and 7. The results were normalized to housekeeping β-ACTIN and were represented as relative fold change to Ti at each time-point. Each condition was done in triplicate ($n = 3$). Each character represents significantly differences respect to the other ones for each time-point (p-value < 0.05).

for C8-HSL (N-(3-Hydroxyoctanoyl)-DL-homoserine lactone) and 3-oxo-C10-HSL (N-(3-Oxodecanoyl)-L-homoserine lactone. In the pre-implantation model, QSMs were also downregulated, however, we note that for GaAg, C14-HSL (N-(3-oxotetradecanoyl)-L-homoserine lactone) was up-regulated.

3.8. GaAg-treated titanium promotes osteodifferentation in hMSC after bacterial inoculation

After 21 days of bacterial infection, both Ag and GaAg-doped samples in co-culture *pre-implantation* were capable of inducing cell mineralization (Fig. 10a). However, no significant differences were found in the percentage of covered area by calcium deposits (Fig. 10b). In-cell western was used to measure protein expression of RUNX2, and SPARC (Fig. 10c), and increased SPARC expression was seen with Ag only compared to GaAg.

In the case of the co-culture *post-implantation*, both doped samples were also able to induce cell mineralization after the bacterial infection (Fig. 10d). No significant differences were found with respect to covered area by calcium deposits (Fig. 10e). As above, significantly more RUNX2 and SPARC expression was noted on Ag surfaces compared to GaAg surfaces.

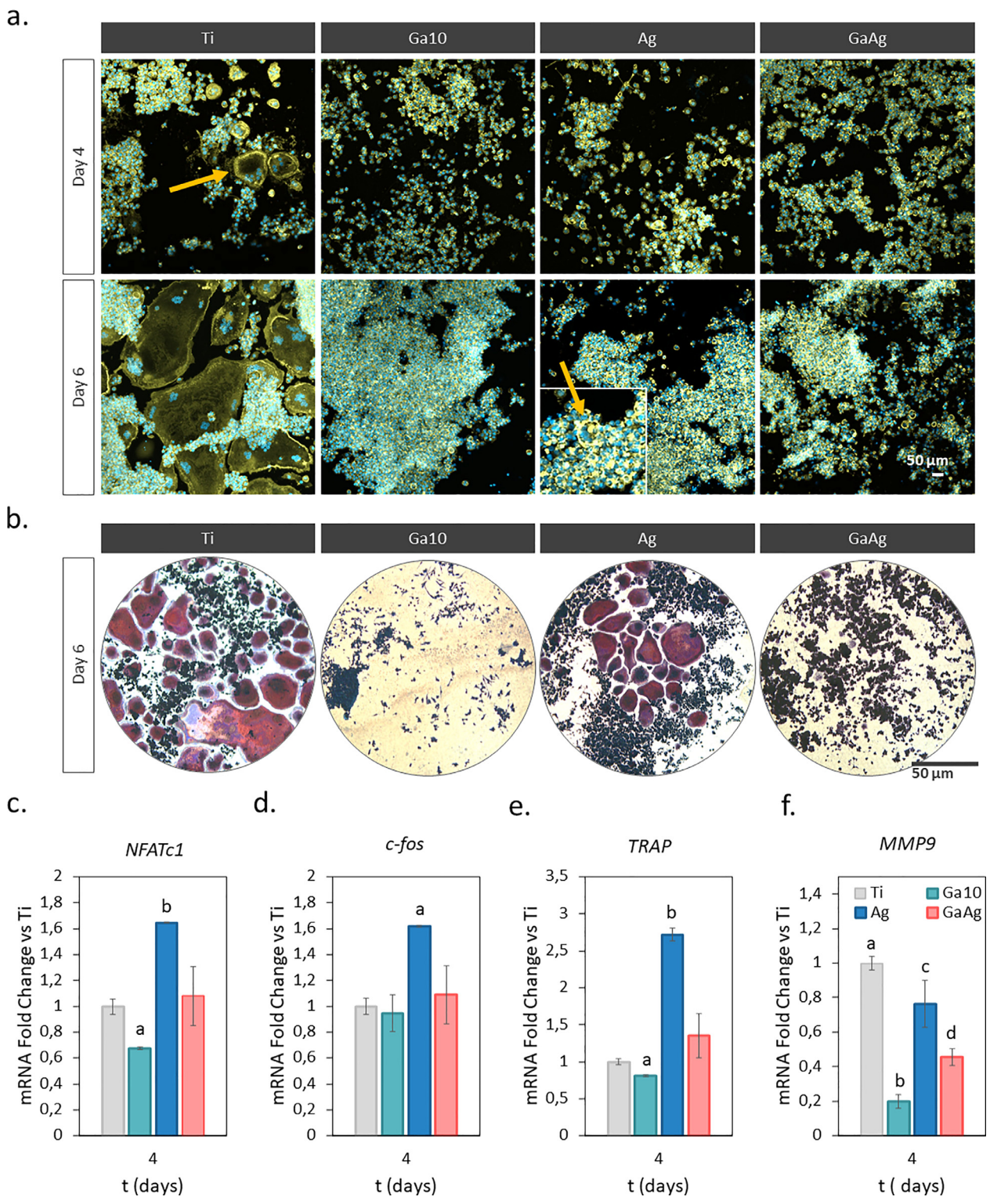

Fig. 5. Effects of Gallium-Silver coating in osteoclastogenesis. (a) Representative images of RANKL-treated RAW264.7 cells after for 4 and 6 days of culture. Cells were labelled with DAPI (nuclei, blue) and phalloidin (F-actin, green). Yellow arrows indicate small multinucleated cells under cell colonies. (b) Representative images of RANKL-treated RAW264.7 cells after 6 days and stained with TRAP. TRAP-positive cells appear colored in violet. RT-PCR analyses of: (c) NFATc1 (d) TRAP (e) c-fos and (f) MMP9 for RANKL-treated RAW264.7 cells after 4 days. The results were normalized using GAPDH as housekeeping and represented as relative fold change to Ti. Each condition was replicated in triplets ($n = 3$). Each character represents significantly differences respect to the other ones for each time-point (p-value < 0.05).

4. Discussion

Several researchers have successfully evaluated the combination of functional ions to improve the performance of biomaterials by providing antibacterial activity with Ag and strontium (Sr) [46], improving bone-bonding properties and anti-meticillin-sensitive *Staphylococcus aureus* activity also with Ag and Sr [47], or enhancing biocompatibility and antibacterial potential with Ga and Sr [48]. In this work, we evaluated the combination of Ag and Ga to reduce the apparition of SSI. In order to achieve this,

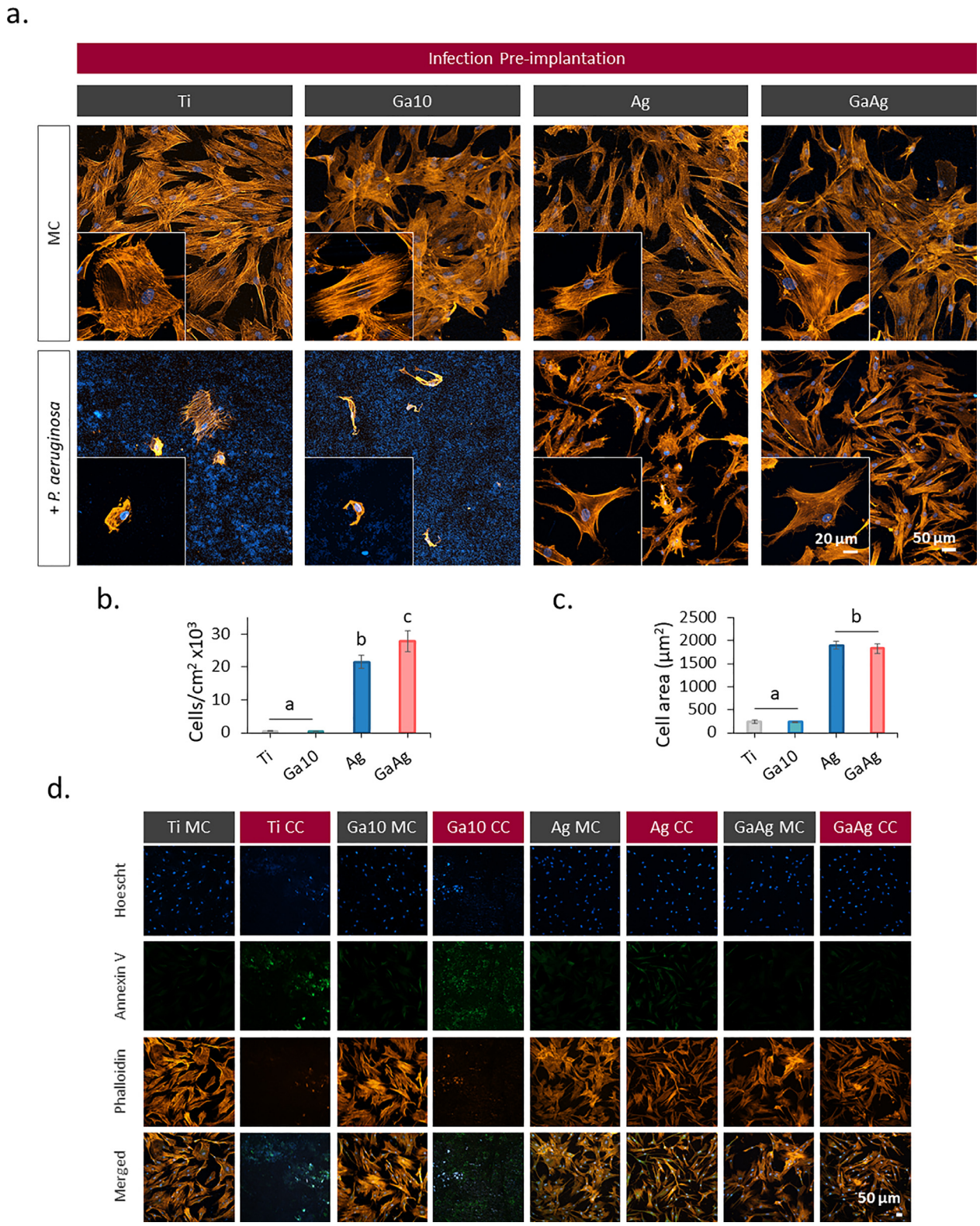

Fig. 6. Infection pre-implantation: cell adhesion, morphology and apoptosis. (a) Representative images of hMSCs in monoculture (MC) and in co-culture with P. aeruginosa by using fluorescence staining. (b) hMSC number per cm^2 in co-culture. (c) hMSC area in co-culture. Each condition was replicated in triplets ($n = 3$) and six images per sample were used for quantification. (d) Representative images of hMSCs in monoculture (MC) and co-culture (CC). Cell nuclei and bacterial DNA were labelled with Hoescht (blue), F-actin with phalloidin (orange) and apoptotic markers with Annexin V (green). Each character represents significantly differences respect to the other ones for each time-point (p-value < 0.05).

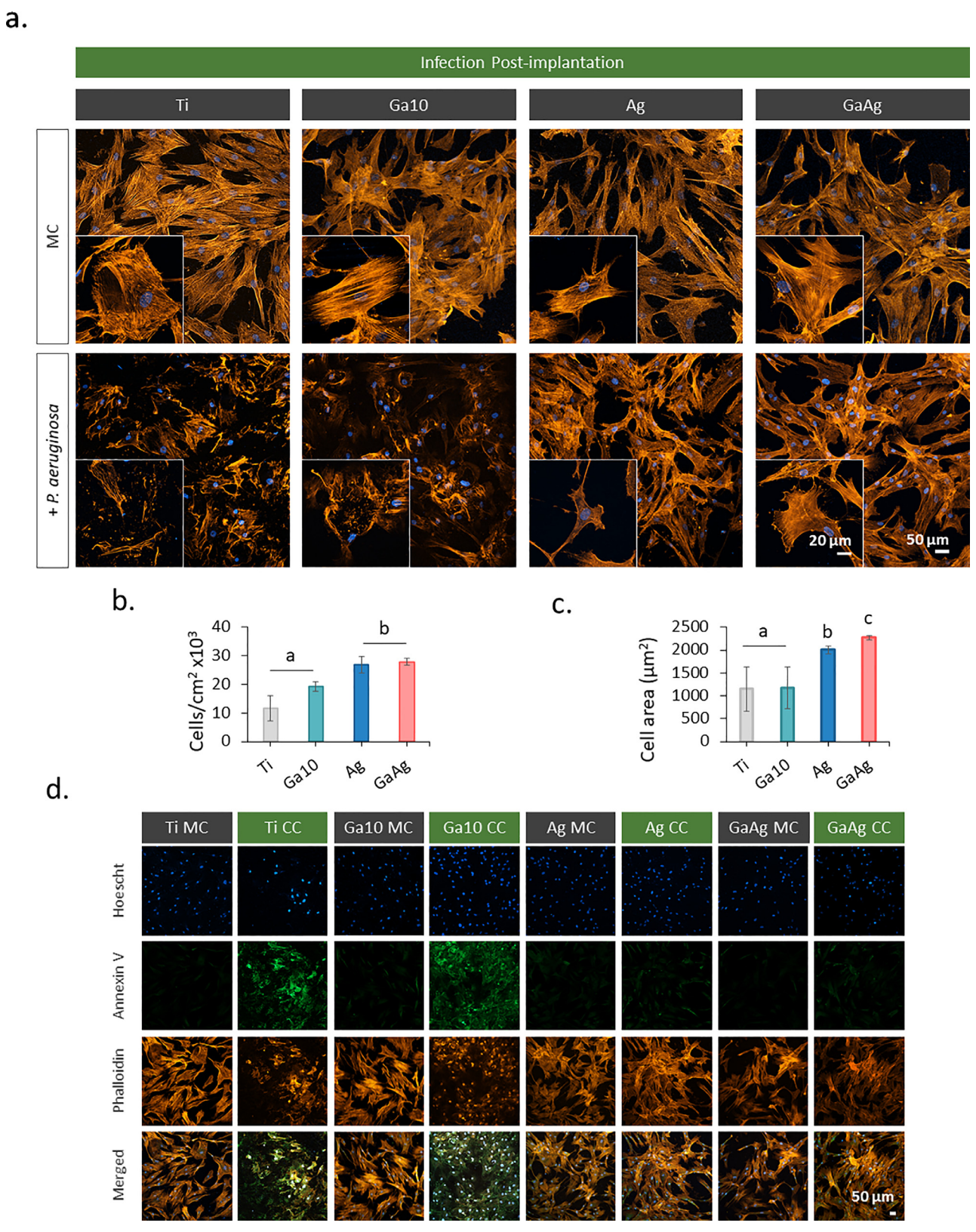

Fig. 7. Infection post-implantation: cell adhesion, morphology and apoptosis. (a) Representative images of hMSCs in monoculture (MC) and in co-culture with P. aeruginosa by using fluorescence staining. (b) Cell number per cm^2 in co-culture. (c) Cell area in co-culture. Each condition was done in triplicate ($n = 3$) and six images per sample were used for quantification. (d) Representative images of hMSCs in monoculture (MC) and co-culture (CC). Cell nuclei and bacterial DNA were labelled with Hoescht (blue), F-actin with phalloidin (orange) and apoptotic markers with Annexin V (green). Each character represents significantly differences respect to the other ones for each time-point (p-value < 0.05).

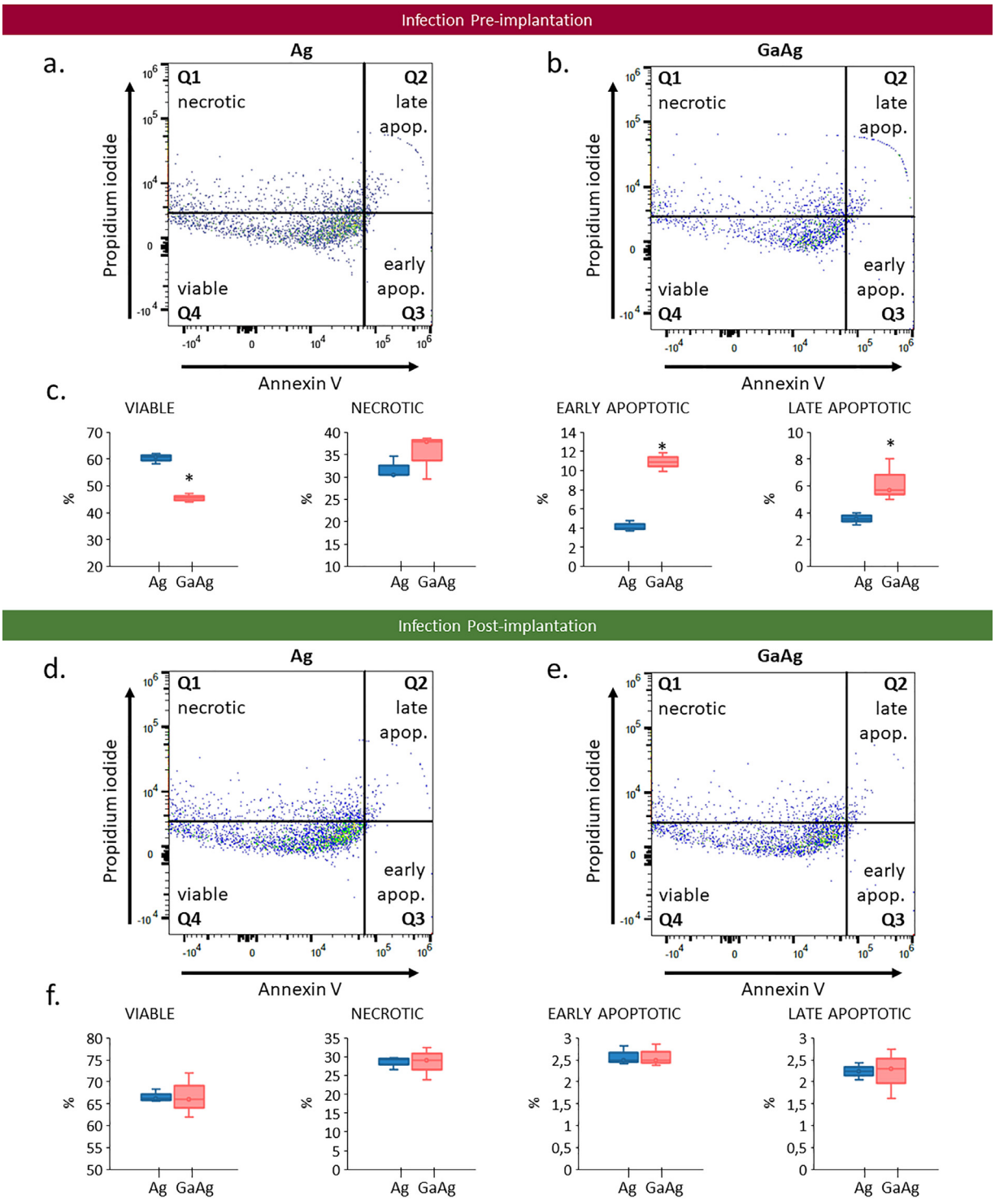

Fig. 8. hMSC viability in co-culture. Gating strategy for flow cytometry analysis for hMSC to be separated on size and viability in the co-culture pre-implantation on the surface of: (a) Ag (b) GaAg. (c) Quantification of viable, necrotic, early apoptotic, and late apoptotic hMSCs after 24 h of co-culture pre-implantation. Gating strategy for flow cytometry analysis for hMSC to be separated on size and viability in the co-culture post-implantation on the surface of: (d) Ag (e) GaAg. (f) Quantification of viable, necrotic, early apoptotic and late apoptotic hMSCs after 24 h of co-culture post-implantation. The gating strategy was the same for all conditions and methods, this figure only shows representative graph of each condition. Asteriks represents significantly differences respect to the other ones (p-value < 0.05).

we studied Ga due to antiresorptive character; and Ag for its antibacterial activity. As a consequence of the GaAg treatment used here, Ag^{+} and Ga^{3+} were capable of being released from the material. In accordance with Rodríguez-Contreras et al. [20], Ag^{+} release was very fast in the first hours in this kind of treatment, however the release of Ga^{3+} was slower and lower. Our results indicate that Ag^{+} is first released from the surface, followed by Ga^{3+}. This matches with XPS data showing that a greater amount of Ag and lower percentage of Ga were found on the GaAg surface. This result seemed to indicate that Ag is found more superficially than Ga. Therefore, Ag^{+} is released first, and then Ga^{3+}.

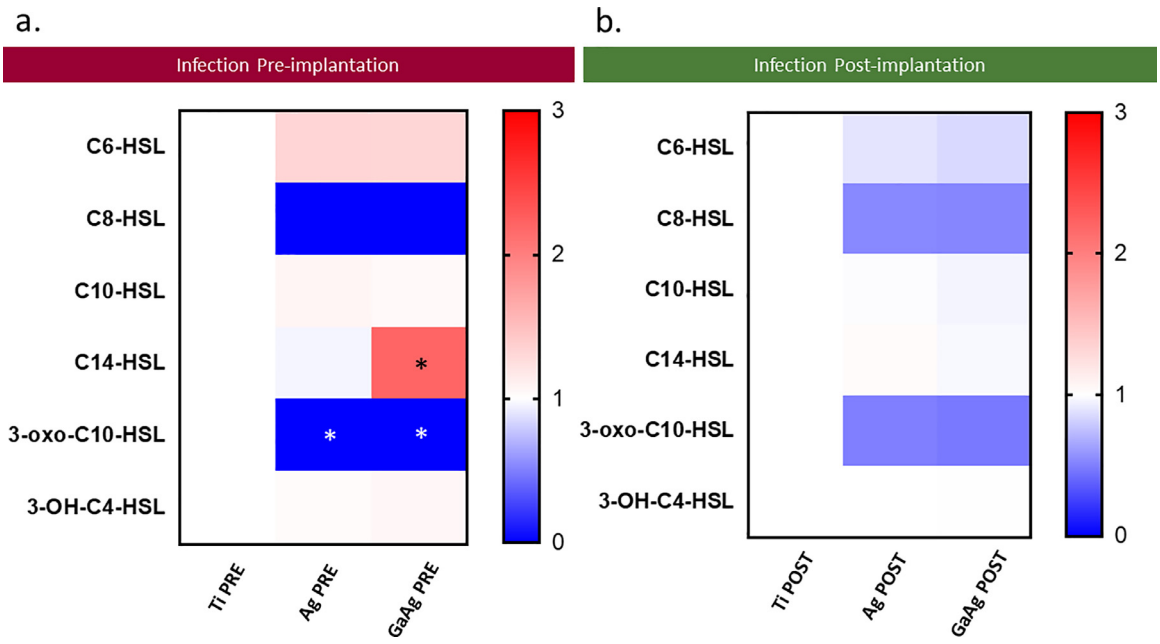

Fig. 9. Quorum Sensing Molecules present in the co-culture. (a) Metabolomic analysis of different QSMs presents on Ti, Ag and GaAg in the method Infection Pre-Implantation. (b) Metabolomic analysis of different QSMs presents on Ti, Ag and GaAg in the method Infection Pre-Implantation. Red indicate up-production and blue down-production respect to Ti. Black and white asterisks represent statically differences respect to Ti. Asterisks represents significantly differences respect to the other ones (p-value < 0.05).

Regarding biological evaluation, hMSC on all conditions looked [49] and grew normally (Fig. 3). However, Ag caused lower cell number and spreading which was recovered by adding Ga. The calcium titanate layer on Ti samples has been reported to enhance osteodifferentiation in many studies [21,50]. Moreover, Ga^{3+} has been reported as an osteoinductive agent [51,52]. In this work, the suitability of calcium titanate and Ga^{3+} to promote osteogenesis was confirmed again (Fig. 4). In addition, with the GaAg combination, the enhancement of mineralization was kept despite the presence of Ag. However, ALP activity, mineralization, RUNX2 and ALP gene expression were significantly lower on Ag only. Although the Ag performance here was inferior compared to Ga10; ALP, mineralization and RUNX2 gene expression were increased compared to Ti control. Even though the improvement in osteodifferentiation by Ag versus Ti was clear, it was probably provided by the effect of calcium titanate. In fact, only few studies have reported Ag^{+} as an ion able to confer osteogenesis [53] but many studies have informed that Ag has no effect [54–56]. Overall, the incorporation of Ga, including with Ag, was shown to be beneficial for hMSC osteogenesis. It is important to note that while Ag itself had no osteogenic benefit, it did not interfere with the benefit, probably due to the effect of the calcium titanate. These results suggested that the mixture retains the suitable osteoinductivity provided by Ga^{3+} and improves those obtained by Ag^{+}. Therefore, GaAg has more ability to induce osteogenesis than Ti and Ag.

According to our anti-resorptive evaluation (Fig. 5), Ga-containing samples inhibited osteoclast formation. However, the GaAg mixture was not able to reduce osteoclast-related genes as strongly as Ga10. Even though its anti-resorptive ability apparently might be reduced compared to Ga only, GaAg samples showed a better reduction of osteoclast genes expression compared to Ag alone. A possible explanation can be that Ag^{+} has been reported as an inductor of osteoclastogenesis by increasing RANKL/osteoprotegerin (OPG) ratio [57]. RANKL and OPG play an important role in osteoclastogenesis since osteoblasts produces RANKL to induce macrophages to differentiate and the process is controlled through the production of OPG, the antagonist [58–61]. Thus, when the RANKL/OPG ratio is increased, osteoclastogenesis is promoted and subsequent bone resorption occurs. Moreover, it is believed that an increase in osteoclast formation may be related to the risk of peri-implant osteolysis [62]. Therefore, not only does Ag enhance osteoclastogenesis but it might also increase the risk of implant failure. However, osteoclastogenesis was significantly reduced on GaAg, showing a profile closer to that of Ga10. Specially, MMP9, involved in bone matrix degradation [63,64], was drastically down-regulated. This result suggested that on the one hand the mixture reduced less efficiently osteoclast formation compared to Ga10, on the other hand, the reduction of osteoclastogenesis was improved compared to Ag, therefore the risk of peri–implant osteolysis would be reduced.

As it was mentioned above, the representation of “the race for the surface” *in vitro* is one of the most realistic approach to evaluate antibacterial activity of a material [65]. Despite this, it is noted that an *in vitro* study has still limitations for its extrapolation to a clinical scenario, since there are several factors, such as the patient’s immune state or the microenvironment surrounded the implant. In this work, the “race for the surface” has been initially assessed without antibiotics in order to prove the antibacterial effect provided by Ag. However, after a certain amount of time, antibiotics were added to protect the surviving cells and provide an appropriate environment to evaluate osteogenesis. Moreover, antibiotics are commonly used in the clinical practice [66] and their use in the *in vitro* study resembles this situation. As it has been described in Piñera-Avellaneda, D. et al. [21], the method for *pre-implantation infection* mimics the scenario in which the implant is inserted in a previously infected bone as in the devastating complication called Periprosthetic Joint Infection (PJI) [67–69]; and the method *post-implantation* represents the situation in which bacterial infection occurs post-implantation due to the patient’s immune-depressed status [70–72]. Our results (Figs. 6 and 7) confirmed that the Ag-doping protected the hMSCs better from bacterial virulence even in combination with Ga. Moreover, samples with Ag provided better hMSC adhesion and protected them from apoptosis [73]. However, although several researchers have

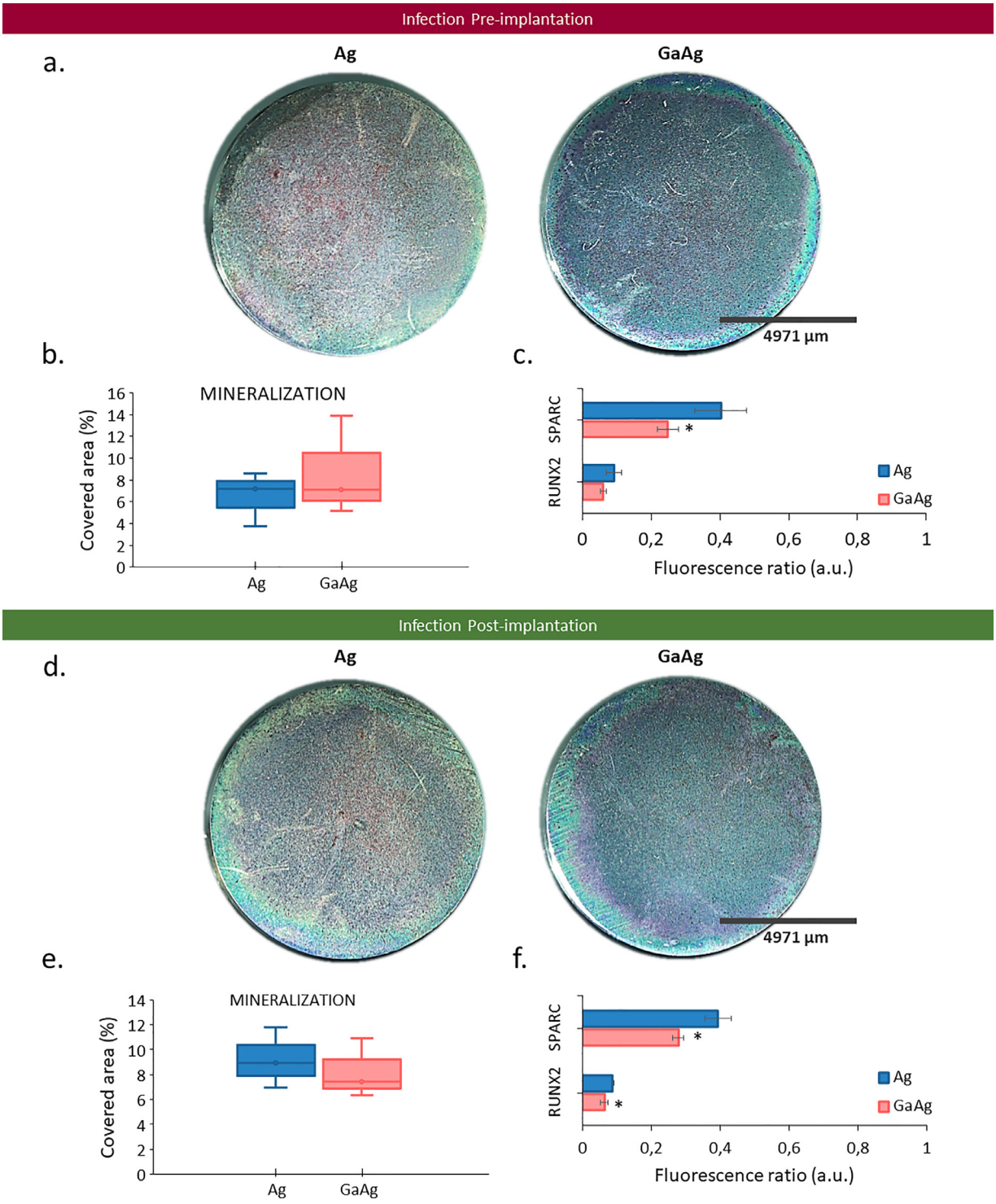

Fig. 10. Osteodifferentation capacity after bacterial infection. (a) Representative images of calcium deposits produced on day 21 in co-culture pre-implantation. (b) Quantification of the calcium deposits in pre-implantation. (c) In-cell western analysis of SPARC and RUNX2 in pre-implantation. (d) Representative images of calcium deposits produced on day 21 in co-culture post-implantation. (e) Quantification of the calcium deposits in post-implantation. (f) In-cell western analysis of SPARC and RUNX2 in post-implantation. Pictures of the whole sample were taken for quantification and calcium deposits were labelled in red using Alizarin Red Staining. Asterisks represents significantly differences respect to the other ones (p-value < 0.05).

successfully proved the antibacterial effect of Ga-based compounds [74–76], especially against *P. aeruginosa* [77–79], the Ga^{3+} released from Ga10 was not enough to kill bacteria in this co-culture system. The results of Figs. 6 and 7 in combination with fig. 8, illustrates that there is not full effect of Ag when included with Ga when conditions are most unfavourable, i.e. in the *pre-implantation model*. However, when the hMSCs populate the surfaces first, both Ag and GaAg offer equal bacterial protection.

In order to understand what was happening in the co-culture, QSMs present inside the bacteria were evaluated (Fig. 9). In the *post-implantation* method, QSMs were present in the bacteria in lesser quantity in the treated samples than untreated Ti, espe-

cially for C8-HSL and 3-oxo-C10-HSL. Both are involved in activation of LasR, a transcription factor involved in biofilm and virulence factor production [80]. In low density conditions, as we have with inclusion of Ag in the Ti surfaces, low bacterial density will result in lowered activation of LasR and can, therefore, be resultant lower bacterial virulence. However, in *pre-Implantation* method, some QSMs were found in higher quantity on GaAg, specially C14-HSL. This molecule is another density-dependant QSM that regulated the LasR and RhlR virulence-control transcription factors [81,82] and has been reported to affect cell viability and induce apoptosis [83,84]. This higher quantity of QSMs could be a reason by which% apoptotic cells was higher on GaAg (Fig. 8). Moreover, it has been reported that *P. aeruginosa* produces QSMs as response to the environment according to bacterial and cell population and the state of the infection [85,86]. In fact, the family of C14-HSL molecules are produced in the phase where *P. aeuriginosa* population is low [87]. Therefore, we hypothesised that these molecules were present on GaAg because the last living bacteria were trying to survive by increasing their virulence more aggressively through the production of these QSMs. Indeed, on Ag were not in high quantity due to the Ag^{+} release here is higher and faster [20] than in the mixture and can kill bacteria more efficiently.

Finally, in order to check if the cells had the capacity to overcome the infection, long-term assays were carried out. After bacterial infection, samples were capable of inducing cell mineralization (Fig. 10). Moreover, both samples promoted the protein expression of SPARC and RUNX2. SPARC, also known as osteonectin, is an extracellular matrix glycoprotein with a pivotal role in bone mineralization [88,89]. These results were in agreement with another work, where hMSCs could also promote RUNX2 expression when seeded on Ti surfaces [90]. Our findings here highlighted that hMSCs were able to recover from bacterial attack and that both Ag-doping samples may stimulate bone regeneration even after bacterial infection.

5. Conclusions

The combination of Ga and Ag in the thermochemical treatment confers great advantages in a non-infected system (mono-culture) by increasing osteospecific differentiation and reducing osteoclastogenesis. In an infection model (co-culture), while GaAg confers little advantage over just Ag, it does not dramatically reduce the effect of Ag. Therefore, it is a good compromise where the surgeon hopes that fast and strong osteoinduction will reduce the probability of infection. However, if infection occurs, the implant retains the strong advantages of Ag. Even though *in vivo* experiments must be carried out, we can conclude that GaAg-treated Ti could become a promising strategy to be applied as osteoporotic and bone tumor prosthesis with high incidence of bacterial infection and thus prevent the apparition of SSI.

Declaration of competing interest

The authors declare that they have no known competing financial interests or personal relationships that could have appeared to influence the work reported in this paper.

CRediT authorship contribution statement

David Piñera-Avellaneda: Conceptualization, Data curation, Formal analysis, Investigation, Methodology, Project administration, Software, Writing – original draft, Writing – review & editing. **Judit Buxadera-Palomero:** Investigation, Methodology, Project administration, Supervision, Validation, Visualization, Writing – review & editing. **Rosalia Cuahtecontzi Delint:** Data curation, Investigation, Methodology, Supervision, Writing – review & editing. **Matthew J. Dalby:** Resources, Supervision, Visualization, Writing – review & editing. **Karl V. Burgess:** Methodology, Resources. **Elisa Rupérez:** Supervision, Validation, Visualization, Writing – review & editing. **José María Manero:** Conceptualization, Funding acquisition, Supervision, Validation, Visualization, Writing – review & editing.

Acknowledgments

The authors acknowledge the Ministry of Science and Innovation of Spain for financial support through the RTI2018-098075-B-C21 project, cofounded by the EU through the European Regional Development Funds (MINECO-FEDER, EU). They also thank the Spanish Government for financial support through PID2021-125150OB-I00 project, as well as the FPI-MEC scholarship of DPA.

References

[1] H. Chouirfa, H. Bouloussa, V. Migonney, C. Falentin-Daudré, Review of titanium surface modification techniques and coatings for antibacterial applications, Acta Biomater. 83 (2019) 37–54, doi:10.1016/j.actbio.2018.10.036.
[2] W. Zimmerli, P. Sendi, Orthopaedic biofilm infections, Apmis 125 (2017) 353–364, doi:10.1111/apm.12687.
[3] J. Josse, F. Valour, Y. Maali, A. Diot, C. Batailler, T. Ferry, F. Laurent, Interaction between staphylococcal biofilm and bone: how does the presence of biofilm promote prosthesis loosening? Front. Microbiol. (2019) 10, doi:10.3389/fmicb.2019.01602.
[4] S. Miwa, N. Yamamoto, K. Hayashi, A. Takeuchi, K. Igarashi, H. Tsuchiya, Surgical site infection after bone tumor surgery: risk factors and new preventive techniques, Cancers (Basel) 14 (2022) 1–12, doi:10.3390/cancers14184527.
[5] J. Meng, Y. Zhu, Y. Li, T. Sun, F. Zhang, S. Qin, H. Zhao, Incidence and risk factors for surgical site infection following elective foot and ankle surgery: a retrospective study, J. Orthop. Surg. Res. 15 (2020) 4–11, doi:10.1186/s13018-020-01972-4.
[6] K. Zhang, Y. Tian, Y. Zhao, M. Tian, X. Li, Y. Zhu, Incidence and risk factors for surgical site infection after femoral neck fracture surgery: an observational cohort study of 2218 patients, Biomed. Res. Int. (2022) 2022, doi:10.1155/2022/5456616.
[7] D. Campoccia, L. Montanaro, C.R. Arciola, The significance of infection related to orthopedic devices and issues of antibiotic resistance, Biomaterials 27 (2006) 2331–2339, doi:10.1016/j.biomaterials.2005.11.044.
[8] A. Sevencan, E.K. Doyuk, N. Köse, Silver ion doped hydroxyapatite-coated titanium pins prevent bacterial colonization, Jt. Dis. Relat. Surg. 32 (2021) 35–41, doi:10.5606/ehc.2021.79357.
[9] E. Christaki, M. Marcou, A. Tofarides, Antimicrobial resistance in bacteria: mechanisms, evolution, and persistence, J. Mol. Evol. 88 (2020) 26–40, doi:10.1007/s00239-019-09914-3.
[10] Z.C. Lum, K.M. Natsuhara, T.J. Shelton, M. Giordani, G.C. Pereira, J.P. Meehan, Mortality during total knee periprosthetic joint infection, J. Arthroplasty. 33 (2018) 3783–3788, doi:10.1016/j.arth.2018.08.021.
[11] T. Hanawa, Titanium-tissue interface reaction and its control with surface treatment, Front. Bioeng. Biotechnol. 7 (2019), doi:10.3389/FBIOE.2019.00170.
[12] M. Kaur, K. Singh, Review on titanium and titanium based alloys as biomaterials for orthopaedic applications, Mater. Sci. Eng. C. 102 (2019) 844–862, doi:10.1016/j.msec.2019.04.064.
[13] A.G. Gristina, P.T. Naylor, Q.N. Myrvik, Biomaterial-centered infections: microbial adhesion versus tissue integration, Pathog. Wound Biomater. Infect. 7 (1990) 193–216, doi:10.1007/978-1-4471-3454-1_25.
[14] T. Kokubo, S. Yamaguchi, Novel bioactive materials developed by simulated body fluid evaluation: surface-modified Ti metal and its alloys, Acta Biomater. 44 (2016) 16–30, doi:10.1016/j.actbio.2016.08.013.
[15] T. Kokubo, H. Takadama, How useful is SBF in predicting in vivo bone bioactivity? Biomaterials 27 (2006) 2907–2915, doi:10.1016/j.biomaterials.2006.01.017.
[16] S. Yamaguchi, S. Nath, Y. Sugawara, K. Divakarla, T. Das, J. Manos, W. Chrzanowski, T. Matsushita, T. Kokubo, Two-in-one biointerfaces—Antimicrobial and bioactive nanoporous gallium titanate layers for titanium implants, Nanomaterials 7 (2017), doi:10.3390/nano7080229.
[17] T. Kizuki, T. Matsushita, T. Kokubo, Antibacterial and bioactive calcium titanate layers formed on Ti metal and its alloys, J. Mater. Sci. Mater. Med. 25 (2014) 1737–1746, doi:10.1007/s10856-014-5201-9.
[18] I. Ielo, G. Calabrese, G. De Luca, S. Conoci, Recent advances in hydroxyapatite-based biocomposites for bone tissue regeneration in orthopedics, Int. J. Mol. Sci. (2022) 23, doi:10.3390/IJMS23179721.
[19] M. Xu, T. Liu, M. Qin, Y. Cheng, W. Lan, X. Niu, Y. Wei, Y. Hu, X. Lian, L. Zhao, S. Chen, W. Chen, D. Huang, Bone-like hydroxyapatite anchored on alginate microspheres for bone regeneration, Carbohydr. Polym. 287 (2022) 119330, doi:10.1016/j.carbpol.2022.119330.
[20] A. Rodríguez-Contreras, D. Torres, B. Rafik, M. Ortiz-Hernandez, M.P. Ginebra, J.A. Calero, J.M. Manero, E. Ruperez, Bioactivity and antibacterial properties of calcium- and silver-doped coatings on 3D printed titanium scaffolds, Surf. Coatings Technol. 421 (2021) 127476, doi:10.1016/j.surfcoat.2021.127476.

[21] D. Piñera-Avellaneda, J. Buxadera-Palomero, M.-P. Ginebra, J.A. Calero, J.M. Manero, E. Rupérez, Surface competition between osteoblasts and bacteria on silver-doped bioactive titanium implant, Biomater. Adv. 146 (2023) 213311, doi:10.1016/J.BIOADV.2023.213311.
[22] P.L. Tran, E. Huynh, A.N. Hamood, A. De Souza, D. Mehta, K.W. Moeller, C.D. Moeller, M. Morgan, T.W. Reid, The ability of a colloidal silver gel wound dressing to kill bacteria in vitro and in vivo, J. Wound Care 26 (2017) S16–S24, doi:10.12968/jowc.2017.26.Sup4.S16.
[23] F. Barras, L. Aussel, B. Ezraty, Silver and antibiotic, new facts to an old story, Antibiotics 7 (2018) 1–10, doi:10.3390/antibiotics7030079.
[24] K. Nešporová, V. Pavlík, B. Šafránková, H. Vágnerová, P. Odráška, O. Žídek, N. Císařová, S. Skoroplyas, L. Kubala, V. Velebný, Effects of wound dressings containing silver on skin and immune cells, Sci. Rep. 10 (2020) 1–14, doi:10.1038/s41598-020-72249-3.
[25] J. Thiel, L. Pakstis, S. Buzby, M. Raffi, C. Ni, D.J. Pochan, S.I. Shah, Antibacterial properties of silver-doped titania, Small 3 (2007) 799–803, doi:10.1002/SMLL.200600481.
[26] B. Li, X. Liu, F. Meng, J. Chang, C. Ding, Preparation and antibacterial properties of plasma sprayed nano-titania/silver coatings, Mater. Chem. Phys. 118 (2009) 99–104, doi:10.1016/J.MATCHEMPHYS.2009.07.011.
[27] A. Kędziora, M. Speruda, E. Krzyżewska, J. Rybka, A. Łukowiak, G. Bugla-Płoskońska, Similarities and differences between silver ions and silver in nanoforms as antibacterial agents, Int. J. Mol. Sci. 19 (2018) 444 Page19 (2018) 444, doi:10.3390/IJMS19020444.
[28] C. Bonchi, F. Imperi, F. Minandri, P. Visca, E. Frangipani, Repurposing of gallium-based drugs for antibacterial therapy, BioFactors 40 (2014) 303–312, doi:10.1002/biof.1159.
[29] C.H. Goss, Y. Kaneko, L. Khuu, G.D. Anderson, S. Ravishankar, M.L. Aitken, N. Lechtzin, G. Zhou, D.M. Czyz, K. McLean, O. Olakanmi, H.A. Shuman, M. Teresi, E. Wilhelm, E. Caldwell, S.J. Salipante, D.B. Hornick, R.J. Siehnel, L. Becker, B.E. Britigan, P.K. Singh, Gallium disrupts bacterial iron metabolism and has therapeutic effects in mice and humans with lung infections, Sci. Transl. Med. 10 (2018) 1–12, doi:10.1126/scitranslmed.aat7520.
[30] D. Piñera-avellaneda, J. Buxadera-palomero, Gallium-doped thermochemically treated titanium reduces osteoclastogenesis and improves osteodifferentiation, (2023) 1–13. https://doi.org/10.3389/fbioe.2023.1303313.
[31] P. Brouqui, M.C. Rousseau, A. Stein, M. Drancourt, D. Raoult, Treatment of pseudomonas aeruginosa-infected orthopedic prostheses with ceftazidime-ciprofloxacin antibiotic combination, Antimicrob. Agents Chemother. 39 (1995) 2423–2425, doi:10.1128/AAC.39.11.2423.
[32] C.A. Ortori, N. Halliday, M. Cámara, P. Williams, D.A. Barrett, LC-MS/MS quantitative analysis of quorum sensing signal molecules, Methods Mol. Biol. 1149 (2014) 255–270, doi:10.1007/978-1-4939-0473-0_21.
[33] M.R. Parsek, D.L. Val, B.L. Hanzelka, J.E. Cronan, E.P. Greenberg, Acyl homoserine-lactone quorum-sensing signal generation, Proc. Natl. Acad. Sci. U. S. A. 96 (1999) 4360–4365, doi:10.1073/pnas.96.8.4360.
[34] A. Rodríguez-Contreras, D. Torres, D. Piñera-Avellaneda, L. Pérez-Palou, M. Ortiz-Hernández, M.P. Ginebra, J.A. Calero, J.M. Manero, E. Rupérez, Dual-action effect of gallium and silver providing osseointegration and antibacterial properties to calcium titanate coatings on porous titanium implants, Int. J. Mol. Sci. 24 (2023) 8762 Page24 (2023) 8762, doi:10.3390/IJMS24108762.
[35] J. Schindelin, I. Arganda-Carreras, E. Frise, V. Kaynig, M. Longair, T. Pietzsch, S. Preibisch, C. Rueden, S. Saalfeld, B. Schmid, J.Y. Tinevez, D.J. White, V. Hartenstein, K. Eliceiri, P. Tomancak, A. Cardona, Fiji: an open-source platform for biological-image analysis, Nat. Methods. 9 (2012) 676–682, doi:10.1038/NMETH.2019.
[36] M. Pičmanová, T. Moses, J. Cortada-Garcia, G. Barrett, H. Florance, S. Pandor, K. Burgess, Rapid HILIC-Z ion mobility mass spectrometry (RHIMMS) method for untargeted metabolomics of complex biological samples, Metabolomics 18 (2022) 1–12, doi:10.1007/S11306-022-01871-1/FIGURES/5.
[37] U. Sharma, D. Pal, R. Prasad, Alkaline phosphatase: an overview, Indian J. Clin. Biochem. 29 (2014) 269, doi:10.1007/S12291-013-0408-Y.
[38] T. Komori, Regulation of proliferation, differentiation and functions of osteoblasts by runx2, Int. J. Mol. Sci. (2019) 20, doi:10.3390/IJMS20071694.
[39] Y. Liu, Z. Wang, M. Ju, Y. Zhao, Y. Jing, J. Li, C. Shao, T. Fu, Z. Lv, G. Li, Modification of COL1A1 in autologous adipose tissue-derived progenitor cells rescues the bone phenotype in a mouse model of osteogenesis imperfecta, (2021). https://doi.org/10.1002/jbmr.4326.
[40] B. Depalle, C.M. Mcgilvery, S. Nobakhti, N. Aldegaither, S.J. Shefelbine, A.E. Porter, Osteopontin regulates type I collagen fibril formation in bone tissue R, Acta Biomater. 120 (2021) 194–202, doi:10.1016/j.actbio.2020.04.040.
[41] P. Collin-Osdoby, P. Osdoby, RANKL-mediated osteoclast formation from murine RAW 264.7 cells BT - bone research protocols, Bone Res. Protoc. 816 (2012) 187–202, doi:10.1007/978-1-61779-415-5.
[42] J. Gohda, T. Akiyama, T. Koga, H. Takayanagi, S. Tanaka, J.I. Inoue, RANK-mediated amplification of TRAF6 signaling to NFATc1 induction during osteoclastogenesis, EMBO J. 24 (2005) 790–799, doi:10.1038/sj.emboj.7600564.
[43] C. Ghayor, R.M. Correro, K. Lange, L.S. Karfeld-Sulzer, K.W. Grä Tz, F.E. Weber, Inhibition of osteoclast differentiation and bone resorption by N-methylpyrrolidone *, (2011). https://doi.org/10.1074/jbc.M111.223297.
[44] M.S. Kim, C.J. Day, C.I. Selinger, C.L. Magno, S.R.J. Stephens, N.A. Morrison, MCP-1-induced human osteoclast-like cells are tartrate-resistant acid phosphatase, NFATc1, and calcitonin receptor-positive but require receptor activator of NFκB ligand for bone resorption, J. Biol. Chem. 281 (2006) 1274–1285, doi:10.1074/jbc.M510156200.
[45] L.H. Stipetic, M.J. Dalby, R.L. Davies, F.R. Morton, G. Ramage, K.E.V. Burgess, A novel metabolomic approach used for the comparison of staphylococcus aureus planktonic cells and biofilm samples, Metabolomics 12 (2016) 1–11, doi:10.1007/S11306-016-1002-0/FIGURES/3.
[46] A. Cochis, J. Barberi, S. Ferraris, M. Miola, L. Rimondini, E. Vernè, S. Yamaguchi, S. Spriano, Competitive surface colonization of antibacterial and bioactive materials doped with strontium and/or silver ions, Nanomaterials 10 (2020) 1–19, doi:10.3390/nano10010120.
[47] K. Masamoto, S. Fujibayashi, S. Yamaguchi, B. Otsuki, Y. Okuzu, T. Kawata, K. Goto, T. Shimizu, Y. Shimizu, T. Kawai, M. Hayashi, K. Morizane, M. Imamura, N. Ikeda, Y. Takaoka, S. Matsuda, Bioactivity and antibacterial activity of strontium and silver ion releasing titanium, J. Biomed. Mater. Res. - Part B Appl. Biomater. 109 (2021) 238–245, doi:10.1002/jbm.b.34695.
[48] M.-S. Song, R.W. Li, Y. Qiu, S.M. Man, D.E. Tuipulotu, N. Birbilis, P.N. Smith, I. Cole, D.L. Kaplan, X.-B. Chen, Gallium–strontium phosphate conversion coatings for promoting infection prevention and biocompatibility of magnesium for orthopedic applications, ACS Biomater. Sci. Eng. (2022), doi:10.1021/acsbiomaterials.2c00099.
[49] F. Haasters, W.C. Prall, D. Anz, C. Bourquin, C. Pautke, S. Endres, W. Mutschler, D. Docheva, M. Schieker, Morphological and immunocytochemical characteristics indicate the yield of early progenitors and represent a quality control for human mesenchymal stem cell culturing, J. Anat. 214 (2009) 759, doi:10.1111/J.1469-7580.2009.01065.X.
[50] A. Rodríguez-Contreras, D. Torres, J. Guillem-Marti, P. Sereno, M.P. Ginebra, J.A. Calero, J.M. Manero, E. Rupérez, Development of novel dual-action coatings with osteoinductive and antibacterial properties for 3D-printed titanium implants, Surf. Coatings Technol. 403 (2020) 126381, doi:10.1016/j.surfcoat.2020.126381.
[51] M. Yu, Y. Wang, Y. Zhang, D. Cui, G. Gu, D. Zhao, Gallium ions promote osteoinduction of human and mouse osteoblasts via the TRPM7/Akt signaling pathway, Mol. Med. Rep. 22 (2020) 2741–2752, doi:10.3892/mmr.2020.11346.
[52] N. Gómez-Cerezo, E. Verron, V. Montouillout, F. Fayon, P. Lagadec, J.M. Bouler, B. Bujoli, D. Arcos, M. Vallet-Regí, The response of pre-osteoblasts and osteoclasts to gallium containing mesoporous bioactive glasses, (2018). https://doi.org/10.1016/j.actbio.2018.06.036.
[53] N. Pajares-Chamorro, Y. Wagley, C.V. Maduka, D.W. Youngstrom, A. Yeger, S.F. Badylak, N.D. Hammer, K. Hankenson, X. Chatzistavrou, Silver-doped bioactive glass particles for in vivo bone tissue regeneration and enhanced methicillin-resistant staphylococcus aureus (MRSA) inhibition, Mater. Sci. Eng. C. 120 (2021) 111693, doi:10.1016/j.msec.2020.111693.
[54] X.Q. Yu, L.X. Xu, Effects of silver nanoparticles on the in vitro culture and differentiation of human bone marrow-derived mesenchymal cells, Mater. Sci. Forum. 852 (2016) 1307–1312, doi:10.4028/www.scientific.net/MSF.852.1307.
[55] A.K. Nguyen, R. Patel, J.M. Noble, J. Zheng, R.J. Narayan, G. Kumar, P.L. Goering, Effects of subcytotoxic exposure of silver nanoparticles on osteogenic differentiation of human bone marrow stem cells, Appl. Vitr. Toxicol. 5 (2019) 123–133, doi:10.1089/AIVT.2019.0001/ASSET/IMAGES/LARGE/FIGURE8.JPEG.
[56] J. Hajtuch, N. Hante, E. Tomczyk, M. Wojcik, M.W. Radomski, M.J. Santos-Martinez, I. Inkielewicz-Stepniak, Effects of functionalized silver nanoparticles on aggregation of human blood platelets, (2019). https://doi.org/10.2147/IJN.S213499.
[57] B.F. Boyce, L. Xing, Functions of RANKL/RANK/OPG in bone modeling and remodeling, Arch. Biochem. Biophys. 473 (2008) 139, doi:10.1016/J.ABB.2008.03.018.
[58] A. Del Fattore, A. Cappariello, A. Teti, Genetics, pathogenesis and complications of osteopetrosis, Bone 42 (2008) 19–29, doi:10.1016/j.bone.2007.08.029.
[59] C. Sobacchi, A. Frattini, M.M. Guerrini, M. Abinun, A. Pangrazio, L. Susani, R. Bredius, G. Mancini, A. Cant, N. Bishop, P. Grabowski, A. Del Fattore, C. Messina, G. Errigo, F.P. Coxon, D.I. Scott, A. Teti, M.J. Rogers, P. Vezzoni, A. Villa, M.H. Helfrich, Osteoclast-poor human osteopetrosis due to mutations in the gene encoding RANKL, Nat. Genet. 39 (2007) 960–962, doi:10.1038/ng2076.
[60] P. Grabowski, Physiology of bone, Endocr. Dev. 28 (2015) 33–55, doi:10.1159/000380991.
[61] T.N. Crotti, M.D. Smith, D.M. Findlay, H. Zreiqat, M.J. Ahern, H. Weedon, G. Hatzinikolous, M. Capone, C. Holding, D.R. Haynes, Factors regulating osteoclast formation in human tissues adjacent to peri-implant bone loss: expression of receptor activator NFκB, RANK ligand and osteoprotegerin, Biomaterials 25 (2004) 565–573, doi:10.1016/S0142-9612(03)00556-8.
[62] J.P. Connors, J.W. Stelzer, P.M. Garvin, I.J. Wellington, O. Solovyova, The role of the innate immune system in wear debris-induced inflammatory peri-implant osteolysis in total joint arthroplasty, Bioengineering (2022) 9, doi:10.3390/BIOENGINEERING9120764.
[63] J.-H. Gu, X.-S. Tong, G.-H. Chen, X.-Z. Liu, J.-C. Bian, Y. Yuan, Z.-P. Liu, Regulation of matrix metalloproteinase-9 protein expression by 1α, 25-(OH) 2 D 3 during osteoclast differentiation, J. Vet. Sci. 15 (2014) 133–140, doi:10.4142/jvs.2014.15.1.133.
[64] J. Guo, X. Zeng, J. Miao, | Chunpeng Liu, F. Wei, D. Liu, | Zhong Zheng, | Kang Ting, C. Wang, Y. Liu, Y. Correspondence, S. Liu, MiRNA-218 regulates osteoclast differentiation and inflammation response in periodontitis rats through Mmp9, (2018). https://doi.org/10.1111/cmi.12979.
[65] S.M. Shiels, L.H. Mangum, J.C. Wenke, Revisiting the "race for the surface" in a pre-clinical model of implant infection, Eur. Cells Mater. 39 (2020) 77–95, doi:10.22203/eCM.v039a05.

[66] S. Veerachamy, T. Yarlagadda, G. Manivasagam, P.K. Yarlagadda, Bacterial adherence and biofilm formation on medical implants: a review, Proc. Inst. Mech. Eng. Part H J. Eng. Med. 228 (2014) 1083–1099, doi:10.1177/0954411914556137.
[67] G. Renard, J.M. Laffosse, M. Tibbo, T. Lucena, E. Cavaignac, J.L. Rouvillain, P. Chiron, M. Severyns, N. Reina, Periprosthetic joint infection in aseptic total hip arthroplasty revision, Int. Orthop. 44 (2020) 735–741, doi:10.1007/s00264-019-04366-2.
[68] Y. Fan, Y. Xiao, W.A. Sabuhi, C.P. Leape, D. Gil, S. Grindy, O.K. Muratoglu, H. Bedair, J.E. Collins, M. Randolph, E. Oral, Longitudinal model of periprosthetic joint infection in the rat, J. Orthop. Res. 38 (2020) 1101–1112, doi:10.1002/jor.24556.
[69] V.W.K. Chan, P.K. Chan, H. Fu, M.H. Cheung, A. Cheung, C.H. Yan, K.Y. Chiu, Preoperative optimization to prevent periprosthetic joint infection in at-risk patients, J. Orthop. Surg. 28 (2020) 1–8, doi:10.1177/2309499020947207.
[70] J.M. Anderson, Future challenges in the in vitro and in vivo evaluation of biomaterial biocompatibility, Regen. Biomater. 3 (2016) 73–77, doi:10.1093/RB/RBW001.
[71] C.R. Arciola, D. Campoccia, L. Montanaro, Implant infections: adhesion, biofilm formation and immune evasion, Nat. Rev. Microbiol. 16 (2018) 397–409, doi:10.1038/s41579-018-0019-y.
[72] A.L. Overmann, C. Aparicio, J.T. Richards, I. Mutreja, N.G. Fischer, S.M. Wade, B.K. Potter, T.A. Davis, J.E. Bechtold, J.A. Forsberg, D. Dey, Orthopaedic osseointegration: implantology and future directions, J. Orthop. Res. 38 (2020) 1445–1454, doi:10.1002/jor.24576.
[73] M. Van Engeland, L.J.W. Nieland, F.C.S. Ramaekers, B. Schutte, C.P.M. Reutelingsperger, Annexin V-affinity assay: a review on an apoptosis detection system based on phosphatidylserine exposure, Cytometry 31 (1998) 1–9, doi:10.1002/(SICI)1097-0320(19980101)31:1⟨1::AID-CYTO1⟩3.0.CO;2-R.
[74] F. Li, F. Liu, K. Huang, S. Yang, Advancement of gallium and gallium-based compounds as antimicrobial agents, Front. Bioeng. Biotechnol 10 (2022) 64, doi:10.3389/FBIOE.2022.827960/BIBTEX.
[75] S.P. Valappil, D. Ready, E.A. Abou Neel, D.M. Pickup, W. Chrzanowski, L.A. O'Dell, R.J. Newport, M.E. Smith, M. Wilson, J.C. Knowles, Antimicrobial gallium-doped phosphate-based glasses, Adv. Funct. Mater. 18 (2008) 732–741, doi:10.1002/adfm.200700931.
[76] F. Minandri, C. Bonchi, E. Frangipani, F. Imperi, P. Visca, Promises and failures of gallium as an antibacterial agent, Fut. Microbiol. 9 (2014) 379–397, doi:10.2217/fmb.14.3.
[77] J.A. Lessa, G.L. Parrilha, H. Beraldo, Gallium complexes as new promising metallodrug candidates, Inorganica Chim. Acta 393 (2012) 53–63, doi:10.1016/j.ica.2012.06.003.
[78] Y. Kaneko, M. Thoendel, O. Olakanmi, B.E. Britigan, P.K. Singh, The transition metal gallium disrupts Pseudomonas aeruginosa iron metabolism and has antimicrobial and antibiofilm activity, J. Clin. Invest. 117 (2007) 877–888, doi:10.1172/JCI30783.
[79] M. Mosina, C. Siverino, L. Stipniece, A. Sceglovs, R. Vasiljevs, T.F. Moriarty, J. Locs, Gallium-doped hydroxyapatite shows antibacterial activity against pseudomonas aeruginosa without affecting cell metabolic activity, J. Funct. Biomater. (2023) 14, doi:10.3390/JFB14020051/S1.
[80] P. Williams, M. Cámara, Quorum sensing and environmental adaptation in pseudomonas aeruginosa: a tale of regulatory networks and multifunctional signal molecules, Curr. Opin. Microbiol. 12 (2009) 182–191, doi:10.1016/J.MIB.2009.01.005.
[81] S.T. Rutherford, B.L. Bassler, Bacterial quorum sensing: its role in virulence and possibilities for its control, cold spring harb, Perspect. Med. 2 (2012), doi:10.1101/CSHPERSPECT.A012427.
[82] H. Huang, X. Shao, Y. Xie, T. Wang, Y. Zhang, X. Wang, X. Deng, An integrated genomic regulatory network of virulence-related transcriptional factors in pseudomonas aeruginosa, Nat. Commun. (2019) 10, doi:10.1038/S41467-019-10778-W.
[83] B.M. Davis, R. Jensen, P. Williams, P. O'Shea, The interaction of N-acylhomoserine lactone quorum sensing signaling molecules with biological membranes: implications for inter-kingdom signaling, PLoS ONE 5 (2010), doi:10.1371/JOURNAL.PONE.0013522.
[84] J. Zhang, F. Gong, L. Li, M. Zhao, J. Song, Pseudomonas aeruginosa quorum-sensing molecule N-(3-oxododecanoyl) homoserine lactone attenuates lipopolysaccharide-induced inflammation by activating the unfolded protein response, Biomed. Reports 2 (2014) 233–238, doi:10.3892/br.2014.225.
[85] C.M. Waters, B.L. Bassler, Quorum sensing: cell-to-cell communication in bacteria, Annu. Rev. Cell Dev. Biol. 21 (2005) 319–346, doi:10.1146/annurev.cellbio.21.012704.131001.
[86] M.F. Moradali, S. Ghods, B.H.A. Rehm, Pseudomonas aeruginosa lifestyle: a paradigm for adaptation, survival, and persistence, Front. Cell. Infect. Microbiol. 7 (2017), doi:10.3389/fcimb.2017.00039.
[87] P. Moura-Alves, A. Puyskens, A. Stinn, M. Klemm, U. Guhlich-Bornhof, A. Dorhoi, J. Furkert, A. Kreuchwig, J. Protze, L. Lozza, G. Pei, P. Saikali, C. Perdomo, H.J. Mollenkopf, R. Hurwitz, F. Kirschhoefer, G. Brenner-Weiss, J. Weiner, H. Oschkinat, M. Kolbe, G. Krause, S.H.E. Kaufmann, Host monitoring of quorum sensing during pseudomonas aeruginosa infection, Science (2019) 366 (80-.), doi:10.1126/science.aaw1629.
[88] J.D. Termine, H.K. Kleinman, S.W. Whitson, K.M. Conn, M.L. McGarvey, G.R. Martin, Osteonectin, a bone-specific protein linking mineral to collagen, Cell 26 (1981) 99–105, doi:10.1016/0092-8674(81)90037-4.
[89] J. Sodek, B. Zhu, M.H. Huynh, T.J. Brown, M. Ringuette, Novel functions of the matricellular proteins osteopontin and osteonectin/SPARC, Connect. Tissue Res. 43 (2002) 308–319, doi:10.1080/03008200290001050.
[90] L.A. Damiati, M.P. Tsimbouri, V.-L. Hernandez, V. Jayawarna, M. Ginty, P. Childs, Y. Xiao, K. Burgess, J. Wells, M.R. Sprott, R.M.D. Meek, P. Li, R.O.C. Oreffo, A. Nobbs, G. Ramage, B. Su, M. Salmeron-Sanchez, M.J. Dalby, Materials-driven fibronectin assembly on nanoscale topography enhances mesenchymal stem cell adhesion, protecting cells from bacterial virulence factors and preventing biofilm formation, Biomaterials 280 (2022) 121263, doi:10.1016/j.biomaterials.2021.121263.